LIDAR HEAT MAP BASED CHANNEL SOUNDING FOR COMPLEX WIRELESS ENVIRONMENTS

James Taylor

B.Eng. (Hons)

Submitted in fulfilment of the requirements for the degree of

Masters of Engineering (Research)

School of Electrical Engineering & Computer Science

Queensland University of Technology

2016

Statement of Original Authorship

This thesis and its contained work has not been previously submitted for the requirements of an award at this or any other higher education institution. It does not to my knowledge contain any material previously published or written by another person that is not referenced in accordance with the IEEE referencing standard.

Signature

Date: 25/2/16

Keywords

LiDaR, Wireless sensor network, WSN, Network deployment methods, RSSI, Static network deployment, Remote sensing, Heat map, RF signal loss.

Abstract

Wireless sensor networks in the 2.4 GHz range are used for the transport and control of sensory data from sensor locations to a central location, either a gateway or sink. A large focus of research in this area is on various methods of power saving techniques pre or post deployment. Pre deployment power optimisations strategies are the most cost effective to implement from a hardware cost perspective. Furthermore a planned deployment method allows for power savings to be made through optimisation of positioning characteristics. The main contribution of this Thesis is the exploration of a new method of signal loss simulation through the manipulation of Light Detection and Ranging (LiDaR) data in the creation of a density profile map, consisting of vertical object coverage. Such a profile predicts the probability of a blockage and therefor a signal loss. This is a large advantage over traditional manual characterisation methods that use static transmitter locations to gain a signal loss between points. Results have shown a correlation between the simulation method and actual measurement. Concluding this a new method for calculating signal loss using LiDaR as the information source.

Table of Contents

List of Figures

List of Tables

Acronyms & Notations

RoI – Region of Interest

QoS – Quality of Service

LiDaR – Light Detection and Ranging

WSN – Wireless Sensor Network

SERF – Samford Ecological Research Facility

STC – Standard Test Condition

AM – Air Mass

GPS – Global Positioning System

CMMBCR – Conditional Max-Min Battery Capacity Routing

Node – Physical hardware element of the network comprised of electronics and software.

MMBCR – Min-Max battery Cost Routing

MTTPR – Minimum Total Transmission Power Routing

RN – Relay Node

TPC – Transmission Power Control

SN – Sensor Node

PDR – Packet Delivery Ratio

SNR – Signal to Noise Ratio

LQ – Link Quality

RSSI – Radio Signal Strength Indicator

Acknowledgments

I would like to acknowledge the support that was received by partner and her commitment encouraging me to finishing what I started. I would like to thank IFE and the HEEM team for providing the opportunity to complete my maters under their umbrella. I would also like to thank my wonderful supervisors Bouchra Senadji, Dhammika Jayalath and David Rowlings. Gratitude extends to Mathew Dunbabin for ideas, advice and technical support expanding my horizons.

Chapter 1

Introduction

Wireless Sensor Networks (WSN) have grown over the past two decades to become an essential tool in the acquisition of data from diverse settings and sensory applications [1]. These applications range from: research, environmental monitoring, industrial automation and control, health monitoring, military, and traffic surveillance [2]. The availability of WSN technology has created wide spread appeal for inexperienced laymen to create wireless networks in a range of microcontroller systems [3]. All WSN's must have an initial design consideration before deployment. During the design phase, the lifetime of the network and its performance matrices are analysed. This assessment outlines hardware specifications and the division scope of constraints to guide the deployment stage.

Strategies used when deploying a WSN affect performance, and additional post-deployment steps to improve flaws in its architecture. WSN designs are considered bespoke through location, inherently creating a non-standardised problem in deployment strategy. In complex wireless environments the identification of signal blockages such as terrain, buildings, trees, shrubs, and general large objects, help to determine the deployment locations of WSN nodes. Consequently, the avoidance of such objects will improve the capacity to communicate uninterrupted in better Line of Sight (LOS) conditions. Software applications available currently use Digital Elevation Model (DEM) maps in conjunction with surface models of

building to calculate and render heat maps of signal loss, One such application is ICS designer by ATDI [4].

The comprehensive body of research conducted in the field of WSN deployment, suggests that there are two main methods of deployment: planned and random [1]. Random deployment is predominately designed to obtain sensory results from a Region of Interest (RoI). A drawback of randomised architecture is its increased density compared to plan deployment. This can be associated with a quality of service (QoS) requirement. Additionally dense networks have a higher equipment cost.

Deployment research identifies planning as the key factor in network routing efficiency [2]. A large proportion of deployment research is based on routing theory and its use in planning for intermediate node locations surrounding RoI. It is widely accepted that such methods will decrease requirements for redundancy and improving overall network routing efficiency. Maximising routing efficiency reduced the energy cost related to nodes. This is a large factor when a node only has a battery for continued operation. Most methods that employ routing theories outline the use of relay nodes (RN) or super nodes (SN). The additions of these nodes act to function as a sub-gateway for a group of nodes. Planned methods of this type rely heavily on mathematical simulations to calculate optimal node placement.

Traditional deployment planning is facilitated by measurements of signal loss conducted through channel sounding. Such methods are predominately used in the commercial sector of WSN deployment. Channel sounding techniques are used to determine a sites signal loss characteristic through a method of injecting a signal into the channel between 2 antennas and measuring the resultant signal. Measurements are repeated in the surrounding area to produce a signal loss map. The granularity of measurements is proportionate to the time taken to conduct the channel sounding process and the quality of the equipment. Channel sounding equipment is expensive and is not accessible to the majority of WSN applications as their installed equipment is not generally high value.

The idea of this research is to replace channel sounding equipment with a single Light Detection and Reneging (LiDaR) scan of the area. LiDaR is defined as a method of measuring distance through the reflection of light from a source point to and object and back. Distance measurements can be compiled to create a 3D map of reflections. Giving an equivalent tool to make planning decisions in the design phase of the deployment. While reducing the cost of the equipment required to obtain such signal loss information. Additional features that this method would provide that surpasses conventional channel sounding is an ability to reposition points of transmission within the map to restimulate and obtain new signal loss maps. Current methods exist in

1.1 Research problem

Research into WSN deployment has highlighted that planned deployment is optimal for network routing efficiency. Current topographical simulation methods like ICS designer [4], are used for network planning, but do not utilise a relationship between signal loss and small-scale spatial objects. Instead they rely on DEM maps and surface information including, average tree height [5]. The capture of small-scale spatial objects through the use of LiDaR and their relationship to signal loss has not been investigated. The use of LiDaR data in this method allows for a close relationship to environmental objects with a dynamic ability to adjust simulation for optimal path planning in a deployment strategy. The significance of this relationship allows for alternate methods of data collection to channel sounding, with more advanced, cheaper tools. A simulation model derived from this research would achieve greater accessibility for users with a faster easer way to generate site's heat map, consisting of planned node locations and signal loss over a spatial area.

1.2 Motivation

The motivation for this research is to identify a method of deployment in a non-heterogeneous environment. A current project at the Queensland University of Technology requires a WSN to

be deployed at Samford Ecological Research Facility (SERF). The network is vital to collect sensory data from soil moisture probes that are in situ at pre-determined locations. These locations will add to the planning scope for the positioning of static nodes at RoI. Additionally, nodes will have the capacity to record other sensory data. The Samford site is considered to be a peri urban bush site with variations in vegetation and train [6]. This site is the ideal setting to meet the conditions of a deployment problem of a non-heterogeneous environment. Additional motivations for the deployment extend from a minimisation in disturbance to the bush environment. Over time human collection from sensors creates tracks into the undergrowth and can result in erosion and/or compaction that will affect the runoff patterns and soil moisture readings.

The method proposed in this research would allow layman to collect the data required to run the model. The model would produce a planned distribution of network elements for small object avoidance, thus creating an increase in LOS conditions.

The WSN will be designed to function indefinitely over the life of the project. This will require an uninterrupted power supply. Due to the location of onsite power, only the main collection point (gateway) can be connected to mains power. Solar power technology is readily available and a suitable replacement for mains power in settings with sufficient sunlight. Sensors in locations below the tree's canopy will have reductions in available light and this shadowing will reduce the ability to regenerate energy, making energy conservation a high priority. Increasing the size of the photovoltaic panels would inherently increase the energy collection properties. However, this is not a viable option due to the accessibility issues for larger equipment. For this reason, the motivation of optimising energy conservation under tree canopy will be the focus of this research, whereby creating methods of improving use efficiency in network systems that will be installed at SERF.

Additional tasks that were overcome as part of this research to achieve the main data collection and part of the network design procedure, were investigated and include:

- Light profiling experiment to obtain light levels below the surface of the canopy. This will be used in conjunction with hardware selection as part of the network planning to calculate solar power panel sizes and hardware power usage constraints (see Appendix A).
- Hardware design and construction, as part of the design phase of the network, the constraints of hardware RF outputs and power conservation techniques were analysed (see Appendix B).

1.3 Objectives

The outcome from this research is a simulation tool that will generate a signal loss heat map for finding key positions using signal loss as an estimator to improve network connectivity and facilitate power efficiency in the design phase. To achieve this outcome an initial survey of signal loss and object interaction will be conducted, providing a means of comparison to signal loss and the comparative point in a LiDaR data set. Research objectives include:

1. To develop a methodology for signal loss interactions between variations of object density in vegetation.
2. To find a method of correlating signal loss to LiDaR data.
3. Derive a simulation tool from objective 1 and 2 to create heat map simulation's using Matlab

1.4 Significance

The significance of this research is found within the simplification that a simulation tool that provides information for planning a WSN. Conventional loss models when used to calculate spacing can only produce an average signal loss. This information is used in spacing nodes appropriately but not effectively. Methods that require the use of expensive equipment to more accurately predict signal loss, like channel sounding are not necessarily accessible to a layman

deploying a low cost WSN. Consequently such factors highlight the requirement for a tool that is accurate yet accessible to low cost deployments. Considering this a tool that would predicts signal loss and aids in mapping sensor location post deployment with only a LiDaR data set would be significant to the WSN community. Additionally this tool is applicable to any wireless network planning stage, where signal loss needs to be mapped cost effectively before network deployment.

1.5 Contributions

This research contributes to the area of WSN planned deployment by focusing on a novel method of planning through the use of LiDaR as a simulation tool. No research has outlined a relationship between RF signal strength and LiDaR density calculations. Similar research has looked at the effect of shadowing of objects with respect to GPS signal strength, as such it was conducted in a real-time comparing GPS signal strength compared to live LiDaR density readings. This research contributes the following:

- Research of a relationship between measured 2.4 GHz RSSI signal loss and ray traced vectors from within a vertical density map, produced using a LiDaR point set.
- Heat map simulation technique using a ray tracing method for equivalent RSSI signal loss in complex wireless environments, using only a LiDaR point set.
- Cross validation technique using GPS referenced Radio Signal Strength Indicator (RSSI) measurements overlayed on simulated ray trace heat map.

1.6 Organisation of the Thesis

The outline of this thesis is as follows:

- **Chapter 1:**
    - Introduction outlining the research problem, motivations, objectives, contributions and the significance of the research.

- **Chapter 2:**
    - Background information on WSN and routing theories, power saving methods, signal loss, LiDaR, energy harvesting, Radio Signal Strength Indicator (RSSI) environment characterisation, LiDaR environmental characterisation and current simulation software.
- **Chapter 3**:
    - Experimental measurement of ground based LiDaR producing a point cloud, acquisition using the Zebedee system by CSIRO.
    - Matlab algorithms to filter point cloud data into a density profile image.
- **Chapter 4:**
    - Object characterisation through transects isolation; profiling three situations of RF signal loss through objects.
- **Chapter 5:**
    - Results section, specifically transect isolations compared with RF channel sounding.
- **Chapter 6:**
    - Discussion, limitations of the system and future research in this area.

Chapter 2

Background information

This chapter provides an overview of literature related to WSNs, LiDaR, LiDaR methods of capture, network deployment methods, network power efficiency, sensor networks, and local power efficiency. Power efficiency can be achieved through several methods, which require understanding of power in its raw form. Power is defined as the rate at which energy is transferred, used, or transformed. In the conservation of energy, any method that can minimise the use, transfer, and transformation of power will increase power efficiency. Therefore, all electrical functions operating on the system have an energy cost. To reduce a cost, the system must have the ability to adapt to become efficient. To identify factors that can improve power efficiency in a WSN, power use functions need to be isolated and understood. A WSN is made up of several main functions that can be considered as system blocks [7].

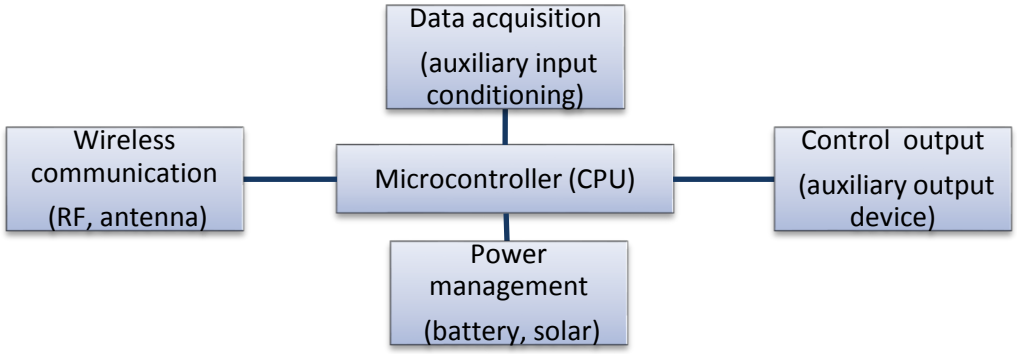

Figure 1 – WSN node function block breakdown for power management elements [8].

2.1 Local node power saving techniques

2.1.1 Energy consumption model

Shnayder et al [9] developed a model to calculate simulated energy consumption of a Mica2. This model measured a Mica2's outputs and compared to simulated results. The measurements (see Table 1) are an accurate representation of the consumption of various components in a Amega128P, a commonly used platform for WSNs. Energy consumption is calculated from current over time. Maintaining lower current modes where possible throughout operation will maximise WSN efficiency.

Table 1- Power model for the Mica2, consisting of current usage for different operation states [8].

Mode	Current	Mode	Current
CPU		**Radio**	
Active	8.0 mA	Rx	7.0 mA
Idle	3.2 mA	Tx (-20 dBm)	3.7 mA
ADC Noise Reduce	1.0 mA	Tx (-19 dBm)	5.2 mA
Power-down	103 μA	Tx (-15 dBm)	5.4 mA
Power-save	110 μA	Tx (-8 dBm)	6.5 mA
Standby	216 μA	Tx (-5 dBm)	7.1 mA
Extended Standby	223 μA	Tx (0 dBm)	8.5 mA
Internal Oscillator	0.93 mA	Tx (+4 dBm)	11.6 mA
LEDs	2.2 mA	Tx (+6 dBm)	13.8 mA
Sensor board	0.7 mA	Tx (+8 dBm)	17.4 mA
EEPROM access		Tx (+10 dBm)	21.5 mA
Read	6.2 mA		
Read Time	565 μs		
Write	18.4 mA		
Write Time	12.9 ms		

2.1.2 Sample time event triggering

Cardell-Oliver et al [10], found physical event triggers could be optimised through the use of a data acquisition block. By lowing the sample rate they could reduce CPU time enabling the extension of node life. Each node had a 1% sleep duty cycle, waking approximately every 12 seconds to communicate with neighbouring nodes. Although savings can be made using this method, the reliability of the SMAC protocol used in a field environment had a packet success rate of 63.8% compared to the 100% experienced in lab testing. Cardell-Oliver highlighted inconsistencies in the node's RF characteristics, noting that link quality varied over the course of a month from very high to very low. Although Cardell-Oliver did not offer a conclusion for

this variation, in such a channel there can be random and non-random noise from RF devices and/or unknown sources.

2.2 Signal characteristics with power efficiency

2.2.1 Channel unpredictability

Pister outlined in a workshop presentation the link quality variations in a Wireless Sensor Network (WSN) [11]. Link quality data from all channels of a 2.4GHz 802.15.4 network were recorded for a period of 27 days. Data analysis suggested that channel stability had an average of 0.9 Packet Delivery Ratio (PDR), however all channels experienced periods of PDR less than 0.4. Pister [11] proposed that in order to reduce dropouts, a WSN needed the ability to hop from one channel to another within its protocols. Furthermore, the resulting increase of PDR would create a reduction in energy cost due to decreased levels of dropped packets.

2.2.2 Dynamic rate adaption

Lanzisera et al [12] suggested that a dynamic rate adaption technique could be used to promote energy reduction. A performance based algorithm that observes previous packets' Link Quality (LQI) and Signal to Noise Ratio (SNR) was used to determine the transmission data rate for upcoming packets and adjust accordingly. This study was conducted on a WSN with 44 nodes and was found to have a 40% average reduction in energy use.

2.2.3 Channel hopping

Watteyne et al [13] suggested that the positioning of a node, in relation to its respective pair, can have an effect on signal quality by demonstrating that link quality can vary from 100% to 0% when moved about a plane 20x35cm (Figure 2). Experimental results supported the model, by demonstrating that by hopping 3 channels the nodes could effectively show the same result as move one node by 5.5cm, subsequently changing the PDR. Additionally, if the hop increases PDR, energy costs for a transmission would drop. As PDR approaches 1 packet error is reduced, directly impacting on transmission time due to less retries.

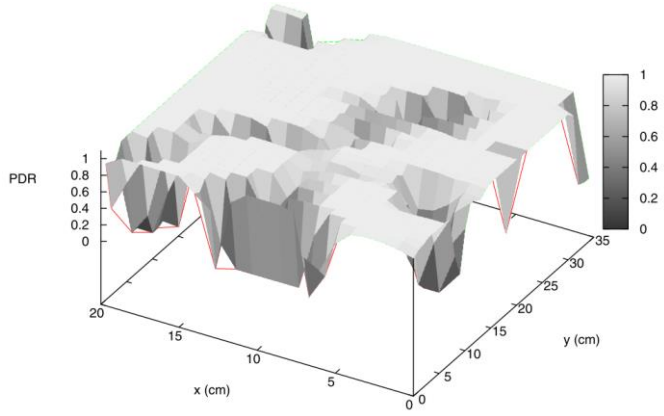

Figure 2 - Packet Delivery Ratio (PDR) test, showing variations in PDR when a node is moved throughout the bounds of a 25cm square test platform [13].

2.2.4 Node placement

Node placement in a WSN can be broken down into critical, Sensor Node (SN), and arbitrary, Relay Node (RN). Applications where a path for a SN cannot reach a gateway along intermediate SN a RN is required to facilitate its communications. Lijie et al [14], suggested that there was an energy efficient method of placing an RN so that the network has linear power consumption throughout the node index. This is obtained through a method of Distance Based Energy Efficient Placement (DBEEP). Accordingly, Lijie [14] demonstrated that simulations efficiency of DBEEP improved by results by157%, in comparison to an equal placement strategy.

2.2.5 Fresnel zone

The Fresnel zone is described as an ellipsoid shaped zone that is used to classify clearance for intermediate object from TX to RX point [15]. If there is an object within this zone, it is possible that the signal will reflect via this object and create an indirect path to the receiving antenna. This can cause a resultant attenuation due to the indirect path phase. There are several Fresnel zones that classify the expanding size of the ellipsoid shape. Each increasing zone has a different loss effect on the received signal. In this experiment there are two cases of Fresnel zone that need to be addressed. The first case considers ground reflectance, due to the RX and TX positions not high enough above the ground along the transmission path. The second case is due to actual objects that are within this zone that are not part of the measurement.

$$F_n = \sqrt{\frac{n\lambda d_1 d_2}{d_1 + d_2}}$$

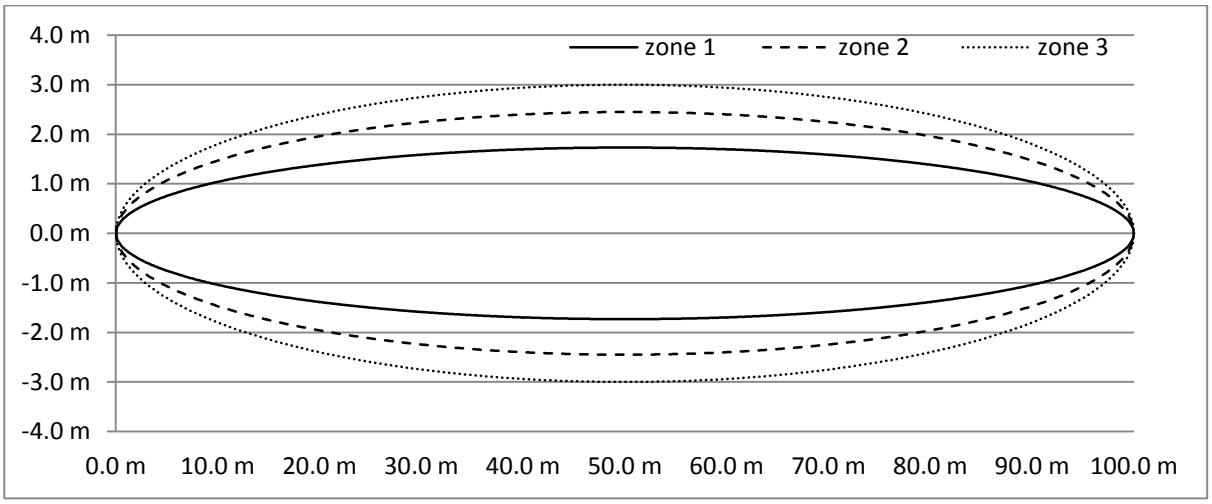

Figure 3 - Fresnel zone plot for zones 1-3 at a distance of 100m and a frequency of 2.4GHz

2.2.6 Path modelling

Quantification of the path loss that the radio signal takes between Rx and TX can be estimated using a range of models. These models are derived from the Free Space Path Loss (FSPL) model that takes into account distance and frequency. More complex models like Empirical direct path model considers obstacles along the transmission path using the multi wall model formula [16], where L_{mwn} is the path loss in dB, and walls between the line of sight are summed and weighted with the value k_i by L_i ;

$$L_{mwn} = L_o + 10n * \log(d) + \sum_{i=1}^{N} k_i L_i$$

This model and the FSPL model are direct path models and do not take into account any influences on the RF signal that incur from reflections creating multi path fading[16]. Such fading of signals at short distances occur in the order of 5-10dB[16].

2.2.7 Transmission power control

Transmission power control in wireless ad hoc networks [17] aim to reduce the total energy consumed in delivery of a packet. Termed as Transmission Power Control (TPC) the technique involves reducing output power of the transmitter while maintaining signal quality. There are two advantages of controlling the power that a node uses to transmit. The first is the ability to

choose who can listen to a transmission, thus increasing the amount of throughput on the network. This feature is limited by nodal relationships as shown in the figure 4;

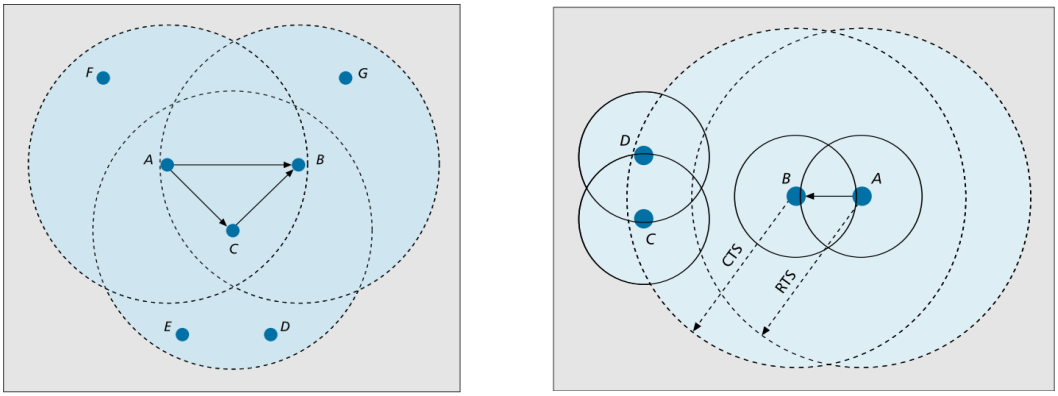

Figure 4 - TPC scenarios, scenario 1 (right), scenario 2 (left) [17]

In scenario one, A can talk to B without affecting transmissions on D or C. In scenario two, there are limited benefits of throughput as the node displacement is roughly even (left) [17].

The second benefit to TPC is the power savings result from reduced transmision power. If A wanted to talk to B it is not nessacary to transmit at maximum power for sucessful communication, thus saving energy. Research has been conducted on this to generate smarter routing protocals [18].

The technique mentioned above, reducing the transmission power for added benefits of the network, can also be integrated into a routing protocol. Studies involving transmission power control in wireless ad hoc networks [17], and a distributed transmission power control protocol for mobile ad hoc networks [18], have found improvements to routing efficiency.

2.3 Network routing

2.3.1 Traditional routing protocols

There are a large number of routing protocols used in WSNs, which vary in fundamental design requirements to provide energy efficiency through the constraints of the application [19]. Sommer [20] identified three different type of routing classifications: proactive (table driven), reactive (on demand), and hybrid (table and on demand). Other protocols that are

common to many systems and widely used in WSNs are; Ad hoc On-Demand Distance Vector Routing (AODV), Dynamic Source Routing (DSR), and Destination-Sequenced Distance Vector routing (DSDV)[21]. AODV and DSR are known as on-demand reactive protocols and only establish a path when a node has a means to send data. DSDV periodically renews the routing tables in spite of the traffic on the network.

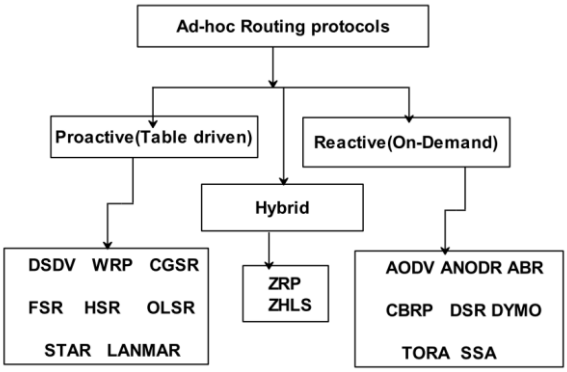

Figure 5 - Routing protocol classification used in WSN's [22].

In a comparative analysis of the three protocols; Cluster Based Routing Protocol (CBRP), AODV and DSDV, it was found that CBRB was limited in situation were the cluster size got too large due to overheads in the per packet increase. Advantages for AODV were noted due to its extremely dynamic nature and use of both unicast and multicast styles of discovery [23]. Disadvantages of AODV were reported in terms of cost, as in comparison to DSR it required more Route Requests (RREQ) for node discovery and path reversal. In addition, there was no reuse of routing information. The DSDV was advantageous as it stores only the best path for a location, instead of maintaining multiple paths, which reduced the overall size of the routing table. Therefore, the protocol guarantees loop free paths. However, a disadvantage of DSDV was the wastage of bandwidth due to periodic routing table updates. DSDV also does not support multipath routing. Increases in network size are proportional to the size of the routing table and therefore the bandwidth usage. Dynamic MANET on-demand (DYMO) is much like AODV in that it is a dynamic protocol. Differing in the generation of a routing table and routing maintenance. This protocol also uses the RREQ model with the addition of route reply

(RREP) and route error (RERR) messages [24]. This protocol is designed to maximise throughput and PDR.

CBRP, AODV, and DSDV are not power aware routing protocols, which use feedback such as battery voltage to adjust their routing paths [25]. In a simulation study [26] three protocol with three approaches to power awareness are analysed. The first study compared, Minimum total transmission power routing (MTPR) involving total power for a given route, with all other possible routes available to the given location, and chose the minimum power path. The second Min-Max battery cost (MMBCR), took into account the battery capacity of each node giving it a numeric value that was weighted in the selection of a route. The third protocol in this study, Conditional Max-Min Battery Capacity routing (CMMBCR), was a hybrid between MTPR and MMBCR. It considered the total path transmission power and remaining battery capacity. From this study it was concluded that MTPR could reduce the total power used by a network, however it can be detrimental to nodes that receive the bulk of the traffic. Despite this, MMBCR outperformed the others in power consumption and increased the lifetime of the total network.

2.3.2 Location based routing

Location based routing utilises a GPS as a tool for aid in routing. This technique was investigated in studies including; a power aware multicasting routing protocol for mobile ad hoc networks with mobility prediction [27], energy-efficient localized topology control algorithms in IEEE 802.15.4 based sensor networks Additionally, this study [28], and energy conserved geo-routing in ad hoc networks [29]. These papers attempted to find a method of using path distances to generate routing tables. Additional benefit of the location based routing was that all nodal clocks could be synchronised from the GPS clock. The energy efficiency of these protocols was found to be up to 60% better than traditional unmodified ad hoc protocols by integrating power awareness and GPS locating [29].

2.3.3 RSSI environment characterization

Recent studies have focused on the use of RSSI (Radio Signal Strength Indicator) as an indicator for environment characterization. One study conducted on localisation, mapped an office using RSSI between two robots with Zigbee access points. The results concluded the granularity of RSSI from the Zigbee was suitable for a means of estimation of link quality [16]. Additionally [16], revealed that transient changes in surrounding environment were indicative of radio propagation models.

2.4 Network redundancy & deployment strategies

Network deployment can be broken up into two overall categories of deployment, random and planned [2]. Each deployment method has a focus based on the WSN requirements. Random deployment aims to capture RoI with individual sensing position less critical to design. Planned deployments use structure-based approaches for positioning. These can be topographical or network based. Redundancy is built into both strategies to overcome faults within the network due to unpredictability including, battery exhaustion and unpredictability in the network channel [30]. Mathematical strategies for deployment fall into four categories including: genetic algorithms, computational geometry, artificial potential field, and particle swarm optimization [2]. These models are aimed at planned and unplanned deployments. However, each model has strong and weak attributes related to deployment characteristics.

2.5 LiDaR

2.5.1 LiDaR

Light Detection and Ranging (LiDaR), or triserial scanning, is defined as a radar like principal, whereby light from a laser is used as the equivalent ranging beam [31, 32]. LiDaR covers a range of systems. A single laser beam is fired from the sensor and the reflected signal is measured, giving distance from the sensor head. By sweeping the laser on a rotational axis, a 2D line of distances is created [33]. Additionally, compounding these 2D lines, by moving the

sensor head in a known direction at a known pace, will create a 3D representation of the sampled space. The output from this 3D system is in Cartesian x, y, z, coordinates, using geo referencing. This can then be converted to real world coordinate systems.

Aerial mounted systems have a return intensity scale that indicated the time for a single beam to return reflected off several elements. This is seen in figure 6.

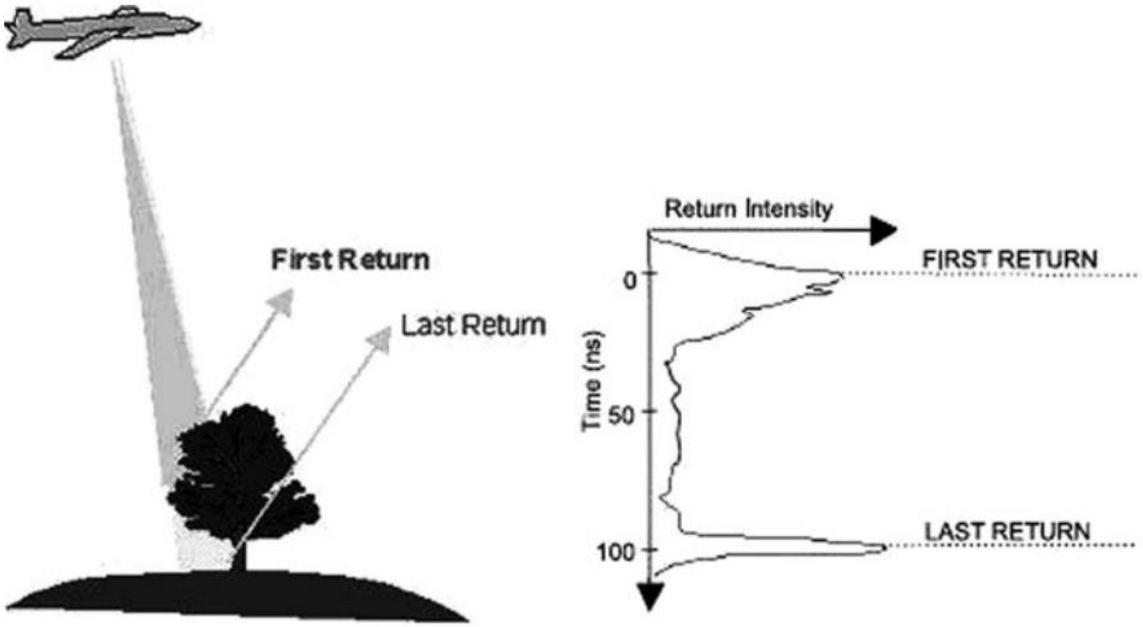

Figure 6 - First and last return example from a Arial LiDaR capture system [32]

Various systems have been developed that use LiDaR. The main application difference is in the secondary and third axis of movement. Arial LiDaR uses three axes and return intensity to represent the reflectiveness of surface. This allows it to distinguish between vegetation buildings and ground surfaces [32, 33]. Vehicle and robot mounted systems generally rotate the laser body on the secondary axis and move the vehicle for the third axis. Reflective intensity is not supported on all of these systems, due to limitations caused by the laser and sensor package used.

CSIRO have recently released a new system of capture, which introduces a variation of motion for the laser. The method is packaged into a device called Zebedee and harnesses the natural motion of a spring for the secondary axis. This motion is excited from the carrying person or vehicle. The third axis is created through the motion of the person or vehicle's trajectory [34].

Figure 7 - UTM-30LX laser used in the production of LiDaR mapping [35]

This system uses a 2D Hokuyo UTM-30LX laser (see figure 7), with a sample rate of 43200 measurements per second. The Zebedee captures raw data from the laser sensor concurrently with an accelerometer and gyroscope found in the MicroStrain 3DM-GX3 MEMS sensor. The data from the MicroStrain is used to calculate the 2nd and 3rd axis. These calculations are done post acquisition due to the complexity and requirement of several samples for the same position [34].

2.5.2 LiDaR environment Characterization

LiDaR is used to characterise environmental features through several methods. Namely the most common method used is in the environmental sciences for surveying. Using GIS applications the data points are separated into layers (i.e. ground and terrain types), and are used to create geographical maps like digital elevation models (DEM)[36]. Other methods of object identification use point formation to define trees and estimate canopy height from live LiDaR data have become more common in robotics.

2.5.3 GNSS characterization with data adding from LiDaR

In 2012 a study called, "GNSS signal multipath error characterization in urban environments using LiDaR data adding" was conducted. This study looked at multipath fading due to objects identifiable through LiDaR and their influence on error characterization. The study found a correlation between vegetation causing multipath fading and signal loss; this was picked up through a synoicous system of measurement with samples taken as the equipment was moved

along the path in the figure below (figure 8). The final outcome concluded that LiDaR caused an increase in the carrier to noise ratio of the GPS signal [37]. Figure 8 shows the study collection path.

Figure 8 - Field data collection path for GPS single loss relationship to LiDaR[37]

2.6 Signal loss Simulation tools

Signal loss simulation tools are used in the deployment strategy for several network architectures. The main focus of such tools is telecommunications, where simulations of cell towers and alike are necessary to gauge customers connection quality. These simulation tools use varying data sets to create diffraction models, absorption models and mixed models [5]. The main focus of defining these models is the path that the signal travels to get to the receiver. If the signal's only option is to travel through an object then it is classified into the absorption model. If the signal is reflected off of a surface and then reaches the receiver then this is the diffraction model. The final model is a mixture of the two. When using the ICS designer software absorption models are used for environmental elements, by isolating vegetative areas in a layer called the clutter layer. This software applies an absorption coefficient to the signal as it passes through these areas. A depiction of mixed model with absorption and diffraction is visible bellow in Figure 9 - Mixed model representation example used in ICS designer [5].

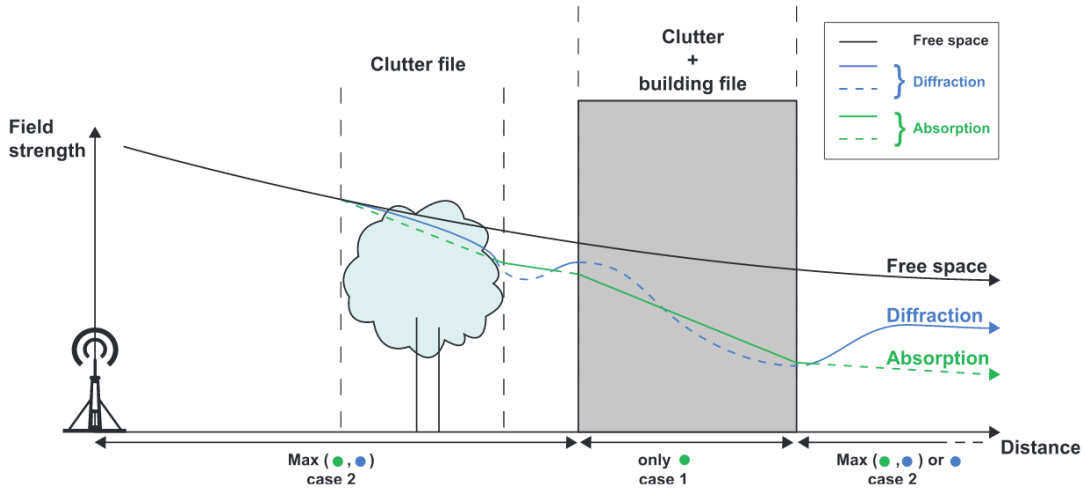

Figure 9 - Mixed model representation example used in ICS designer [5]

2.7 Background summary

This chapter addressed several features associated with power efficiency from local efficiencies to network routing efficiencies. Power efficiency is a critical element in operating a battery reliant network. Planning network elements to have power efficacy through optimal communication links leads to better SNR values and the ability to access transmission power control. To obtain optimal communication links software simulation tools or channel sounding techniques can be used.

Chapter 3

Experiment 1 Measuring Ground Based LiDaR

The literature review highlights methods for the collection of LiDaR. In this chapter the acquisition of this data will be conducted at two sites. The data will then be transformed into a 2D matrix of values. This method of conversion is the key to the creation of a density profile, used for signal loss calculations. For a reduction in site complexity, a preliminary site located on campus has been chosen. This site will be used to conduct the bulk of the testing and calibration of the simulation tools.

Preparations for this experiment involved researching methods of density map creation. This was taken into consideration to understand outcomes. There are several methods for generating a density map. The most common is in the ecological sciences field, in which manual measurements from surveys are carried out by hand, measuring trees and using specific models to give leaf density and canopy coverage [38]. The next level that automates this method is the use of an instrument that calculates the same densities of leaf and canopy, such as a LAI-2200C Plant Canopy Analyser [39]. However, both models are estimations based on an area average or along a transect. The sparseness of data points produced from both methods would not support the expectations for this research. The final method of environmental density mapping is the use of LiDaR. LiDaR captures a high density of information pertaining to

surfaces within the sampled location. For this reason LiDaR was chosen in this experiment for the capture and creation of a density map.

3.1 Aim

This experiment aims to quantify environmental information from two locations by generating a point cloud representation. The first location is adjacent to QUT in the Botanic gardens and the main site of motivation at SERF. Acquiring a spatial data set of the environment with significant detail to prove a correlation of signal loss through point density will be achieved through LiDaR a method of environmental digitization. The LiDaR system used is the Zebedee, created by CSIRO. This hand held laser scanner uses complex positioning algorithms to calculate laser reflections through a spring in motion along a vector; with post processing producing a point cloud of reflected distances. The clouds formatted in the x, y, z, coordinate system. This method was chosen over aerial LiDaR due to a higher capture resolution. Additionally, it estimates blow canopy surfaces with greater detail than an aerial LiDaR. The limitation that this system offers is its retail in returns and hence ambiguity of surface description. Unlike aerial LiDaR the Zebedee returns no reflectance value for a surface.

For the purpose of repetitions and variability three areas will be scanned in this experiment. The first area is in the Botanical gardens of Brisbane city. This area is chosen as it is close to the research area and has varying types of vegetation. Specifically, the first location is one that has an open grass area that has sparsely located tress that will provide the blocks between the two antennas. At the same time keeping complexity to a minimum so that initial results can be seen in the data. The second area is an atypical riparian forest that is located at the SERF facility. This area covers three locations where sensors will be ultimately positioned irrespectively of the networks configuration. The third area to be scanned will be the control area that is an open field that has only grass cover. This area will be defined as a zero density area. The edge of this area is a transition from zero density to a bush forest.

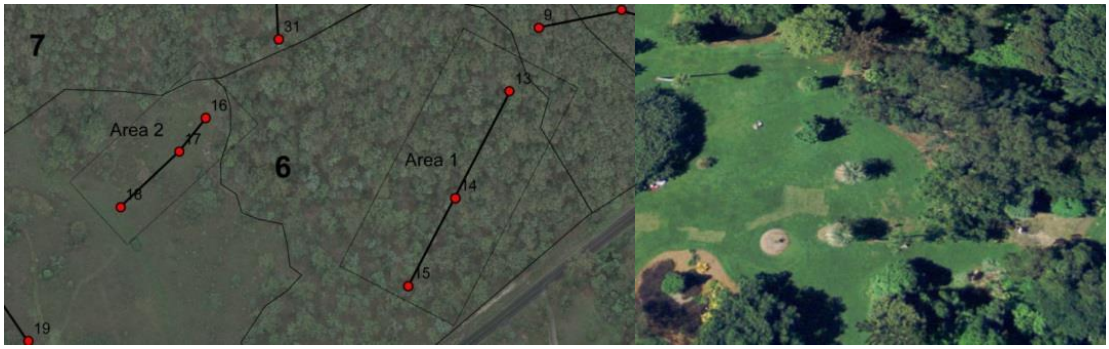

Figure 10 - Area 1 & 2 SERF (left), Botanic gardens site (right).

The second experiment will also capture link quality from the third site, the botanical gardens highlighted above. This data will be produced by using channel sounding methods; whereby, a signal is generated and the response signal is captured by the receiving device. Wide ranges of hardware are available for this and have varying degrees of accuracy and error. Not all of these hardware devices can obtain the data in such a way that it can be logged and geometrically referenced at the same time.

3.2 Zebedee methodology

The Zebedee is a variation on a LiDaR device, varying in its capture technique from standard fixed point LiDaR that are attached to a moving object (i.e. a plane or a motor vehicle). The Zebedee utilises a natural spring motion oscillated through the movement of the users arm to spread its laser beam over its capture area. This motion makes it most useful in areas not accessible by a vehicle. The readings are produced from a spinning laser in the head of the tool, which capture the reflected beams and calculate distance from the time taken. For best results it is recommended to walk in a way that allows the capture head to see all sides of an object through its 180^0 field of view; hence a back tracking method retracing paths in the reverse direction captures all faces of an object. This raw data is normalised through submission to a data server that calculates and removes noise and fragmentation. The data set that is produced by server is defaulted to 4cm gridded points on an XYZ plane scaled in metres. The resolution is also available at 1cm points on request. The plane is zeroed around the start point of the captured run. Through using geo-referencing the data can be shifted to a

UTC style grid system of the measurements. The point cloud that is generated is envisaged as all reflective surfaces within the capture area.

The Zebedee was loaned from CSIRO; the unit comes with a laptop and battery pack in addition to the hand held unit. A custom cable was used to connect the laptop and battery to the laser scanner head. This cable consists of two USB cables that sonorously record data from each of the on board sensors in the system. The computer runs custom acquisition software with a web interface that is accessed through Wi-Fi. Connecting a Wi-Fi enables device like a smart phone to the network and opening the webpage of the device gives access to the controls. The method of acquisition is as follows;

1. The Zebedee sensor is placed on the ground with the laser facing towards the sky. This calibrates the gyroscope sensors. Once a beep is heard from the laptop the sensor is ready to pick up and capture.
2. Picking up the sensor and proceeding to excite the head of the system by moving your arm in an up and down fashion begins the capture.
3. While maintaining the sensors sprung motion, the person holding the sensor moves around the area to be captured in a concentric pattern as to capture surfaces from all angles.
4. Once the capture is completed the sensor is taken back to the zero point where it was calibrated and placed in this same position while the run is finalised on the device that was used to access the Wi-Fi interface.
5. The data is then copied to a USB and sent to CSIRO for processing. The returned data is in ".xyz" format.

3.3 Data filtering method

The data produced in the scanning method is downloaded to a USB to be uploaded to a shared file linked to a CSIRO server that will process the raw data eliminating any points generated by the user moving the scanner. The output file is then downloaded from this server. The files

are returned as a list of Cartesian coordinates each of which representing a return. The Cartesian plane's zero point is referenced from the start point of the capture in the calibration step of the Zebedee capture method.

It was hypothesised that the points representing objects in the point cloud had a relationship to signal attenuation. To characterise the attenuation of RF signal though the points a simulation will be run. The method simulation will retrace a transmission along its interception of object represented in the points as it moves away from TX point. This was referred to as a method of Ray Tracing. The antenna that will be used in the second experiment is an Omni directional antenna. This antenna propagates a radial signal path at 90^0 to plane of the antenna. If the antenna is placed in a vertical position the propagation path will be predominantly horizontal. Additionally, some RF energy is emitted at the top and bottom of the antenna; this will not be taken into consideration, as the antennas will not be mounted in a horizontal position. The major path of signal propagation was considered in this study. Additionally, this simulation will build on a direct path model so no reflections to accommodate for multi-path fading. The Ray Tracing method will show values of signal loss over increasing distances from the transmission point. The following steps will be performed to filter the point cloud;

1. Select relevant points in the propagation plain. from the point cloud
2. Compress points to a 2D matrix.
3. FSPL is subtracted.
4. Ray Trace algorithm simulated from transmission point.
5. Heat map conversion of resultant matrix.

The first step in this method is to select points from the point cloud relevant to the current simulation. This is achieved by considering the points that are 90^0 to antenna at the transmission point. The point group selected will be classified as a slice. The slice will be varied in height and depth in relation to the antenna height as a zero reference. This variation in the slice depth will be studied to uncover the effect of increasing available points in relation

the model's needs and outcomes. Slice equation filters coordinate points of the array where values of z in the range given by a either side of the antenna position (Ant_0)

$$S = \{(x, y, z) | (Ant_0 - a) < z < (Ant_0 + a)\}$$

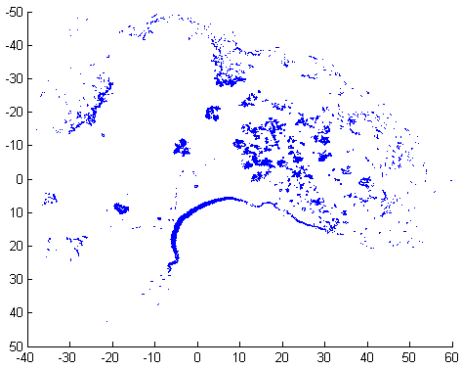

Figure 11 - Top Down view of point cloud XYZ Slice from botanic gardens site.

Figure 12 - Comparable Google Earth Image of figure 11, the same site rotated to same orientation.

The slice (figure 11) then is compressed in to a 2D plane by adding all points in along the Z plane. For simplicity the Z plane is maintained parallel to the antenna plane. This summation gives an estimation of vertical density through the slice. This method assumes signal loss of small object have low Z values. Large dense vertical objects have high Z values, figure 13. Additionally, any object that has a value equal to the slice bounds would be consistent with a solid object and should have a significant effect on signal.

$$\boldsymbol{S_z} = \sum_{i=1}^{Z_n} \boldsymbol{S}_{x,y(i)}$$

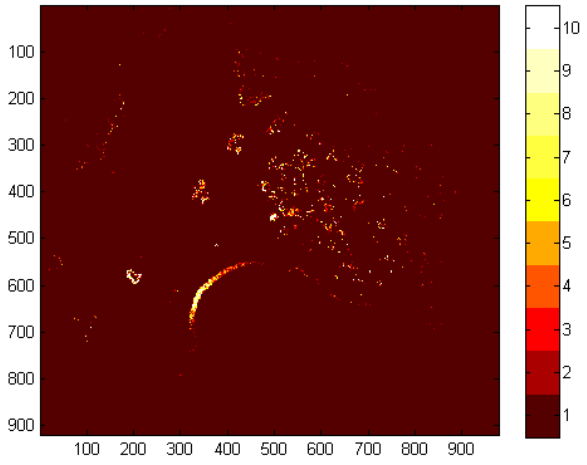

Figure 13 - 2D point density map of botanic gardens site

The 2D slice S_z is a map of density with weighted values for longitudinal objects. This will have a greater indication of object types that have a greater mass, rather than a leaf that will have less impact on the signal attenuation. S_z will serve as a simulation data set allowing any point in the area to have a heat map simulation with the Ray Tracing method.

The Ray Tracing method will represent the signal loss emanating from the point of simulated transmission. Thus, the Ray Tracing equation is built upon the empirical direct path model. This model uses a standard FSPL and a constant to subtract signal loss through walls. The constant in the simulation will be taken from the S_z map during the Ray Trace. The effect of the density point from S_z will be weighted and calibrated against the sampled data from channel sounding in the second experiment. The equation for each Ray is given by R_{dB}, were d is distance in metres, f_{MH} is the frequency of the signal simulated in megahertz, and D the coefficient that is given by the summation of all points along the vector for the given distance;

$$R_{dB} = \ 20 * \log_{10} d + 20 * \ \log_{10} f_{MH} - 27.55 - \ D$$

$$M_{FSPL} = \ 20 * \log_{10} d + 20 * \ \log_{10} f_{MH} - 27.55$$

$$D_{Rt} = D$$

$$\therefore$$

$$R_{dB} = M_{FSPL} + \ D_{Rt}$$

For simplification of the simulation the M_{FSPL} element of this equation is conducted last. Firstly, the Ray Tracing coefficient map D_{Rt} is calculated. This process starts with the blank matrix D_{Rt}, having the same dimension as S_z. All elements in the matrix D_{Rt} are then given the value of the hardware's minimum transceiver sensitivity in dBm. Therefore, the Ray Trace will stop when the maximum dBm is reached. A transmission point of x, y as desired is given, conditionally within dimensional range of S_z. The Ray Tracing method works in a circular motion with a starting angle Θ starting from zero degrees, along the horizontal plane of the 2D map. Each vector starts at point x, y and extends to the edge of the matrix then shifting defined step size to the next Θ value and repeating the process until Θ equals 360 degrees. Each vector is given an initial transmission power in dB, by L_{dB}. As vector passes through each Cartesian

coordinate set it looks up the corresponding position on the S_z matrix for a density value. This value is weighted and subtracted from the running total $L_{dB.}$ The value is inserted in the matrix D_R seen in figure 14_t; the ray will cease when L_{dB} is equal to the hardware's minimum transceiver sensitivity.

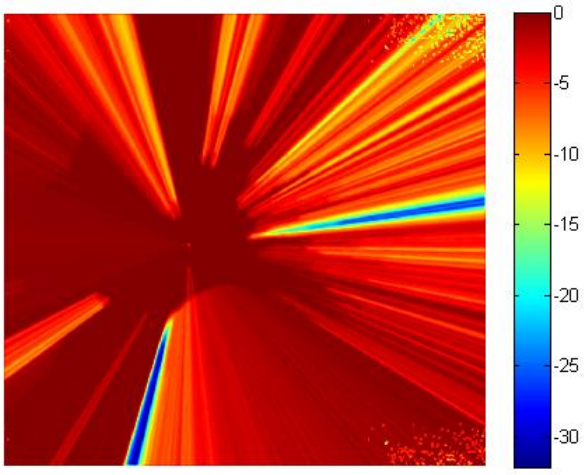

Figure 14 - Ray Trace of botanic gardens site, this matrix is also referenced as D_{Rt}.

The final step is the subtraction of the FSPL element. This is achieved by creating a matrix that has the same dimension as D_{Rt} called M_{FSPL} shown in figure 15 and 16. A transmission point is given using the matching x, y coordinates as above; using a scale of the point cloud each Cartesian coordinate is given a distance X from the point x, y. The whole matrix is then elementally substituted into the FSPL equation for distance to give the below image. The final step in the method is to subtract D_{Rt} from M_{FSPL} to give R_{dB}.

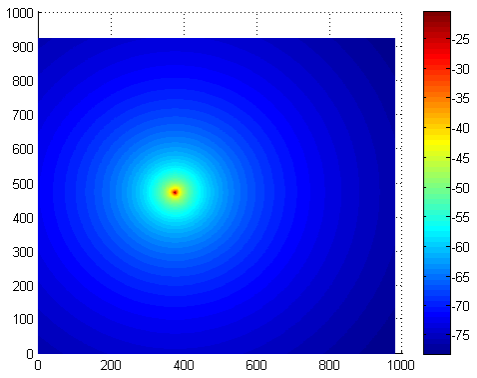

Figure 15 - M_{FSPL} matrix for X, y mirroring Ray Trace's location and size.

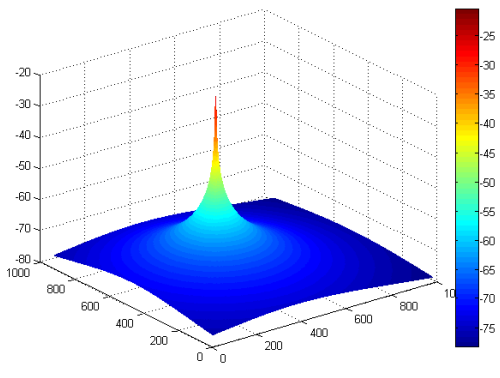

Figure 16 - M_{FSPL} matrix for X, y (3d).

3.4 Results

The initial simulations, without statistical calibration from experiment two, demonstrate that this method can illustrate path loss from any point within the sampled area from the Zebedee. The figure below is the resultant heat map. It can clearly be seen where denser objects are present and have rendered a shadow like effect for signal beyond the object.

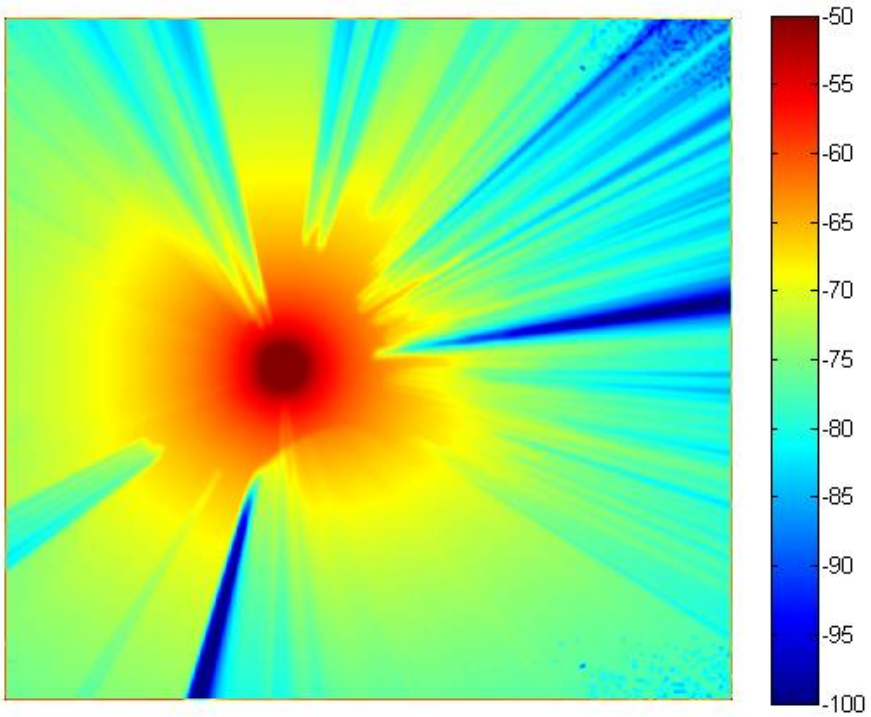

Figure 17 – Heat map output example simulation of M_{FSPL} - D_{RT} an uncelebrated simulation of the botanical gardens full site.

3.5 Limitations

This process has inherent limitations due to the simulation method; these are present in two aspects: quality of the simulation results and simulation time. The final simulation image shows a pixel like effect in the top right hand corner. This effect is due to the sample size of the Ray Tracing method. At the full extension of the trace, the space between each concurrent

trace becomes greater, resulting in missed pixels. By increasing the trace count to adjust for this gap the simulation time inherently increases. The above simulation took an average 16 seconds for a 1000 by 1000 matrix to be simulated on a standard Pc or laptop. Initial simulations were 10 times this amount when sampling to remove all pixilation. Improvements to both time and pixilation could be made to the simulation by exporting the code to a more efficient platform like C++.

3.6 Experiment 1 summary

This experiment was successful in obtaining a data set using the Zebedee tool from two locations, SERF and the Brisbane city botanical gardens. By filtering this data down to a 2D plane across the Z axis a map of vertical density was produced. This map was then combined with a rendering of FSPL using a consistent spacing value as the density map. Subtracting the FSPL map from the density map produces a representation of the models function prior to calibrating it with actual data. The next chapter will look at methods of segmenting data from this density map to produce a comparison of signal loss to summed density loss emanating from the transmission point.

Chapter 4

Experiment 2 RSSI object characterisation

In this chapter an experiment will be conducted in the collection of RF signal loss data through RSSI. The collection of this data is essential to finding a relationship between the LiDaR density map of chapter three and signal loss resulting in the final simulation tool. To perform the subsequent analysis between the two data sets, a method of isolating features in the density map and recoding corresponding RSSI will be covered.

4.1 Aim

The point cloud produced by the Zebedee captures surfaces of a physical environment, representing all objects with a reflectance from the laser. This covers a wide range of physical objects. Relating this to a RF channel, all physical objects have their individual characteristics and intrinsic factor. A model that could classify all objects from the point cloud would be ideal to generate an accurate estimation of signal loss. However, the LiDaR data has limited object information. Methods of capture have varying levels of detail, from none to details about return rate indicating reflectance of an object. To overcome this, it is proposed that a relationship exists between point cloud density and signal loss. To support this, an experiment will be conducted to measure signal attenuation through relative objects present in a point cloud of the same object. This will be achieved through the use of RF equipment with a method of placing transmitting and receiving equipment in various locations and measuring

RSSI. Results from this method will be normalised and correlated point densities for factor of signal loss.

The compressed S_z map from the first experiment will be reviewed to identify a method of data collection in this experiment. Firstly, it was assumed that as the density value increases and approaches the maximum density value for a slice depth, a vertical object is present for the length the slice. This supports the assumption that the S_z plane is a measure of an object that is present in the vertical plane. If an object is present for the length of the vertical plane then the entire RF signal propagated through this point must pass through all objects represented in the density number.

A channel sounding method, with respect to RSSI, will be employed to estimate signal loss to vertical plane density. This is done through estimating different types of vertical density rationalised by objects from the density map, such as open air, leaf material, branches and vertical tree trunks. Measurements of loss via RSSI projected beyond these objects will be collected and cross-referenced with grid positions of equitant RX observations. Next, they will be placed along vertical classification estimation for each degree of density and a profile curve provides an estimation equation for the signal loss relationship D_{RT}. Isolating the loss associated with obstructing objects is calculated by subtracting M_{FSPL} from R_{dB} to give D_{RT}. The equation for M_{FSPL} would then calibrated to the hardware used in the subsequent testing.

4.1.1 Site selection

The botanic gardens site was broken up in to three sites to represent different types of objects with various vertical density grades.

Site 1 represents two types of vertical density within one object, a tree seen in figure 18. The broad leaves and medium sized trunk of the tree allows for simulation through purely leaf material and an additional leaf trunk composite. This object represents medium to high vertical density for S_z.

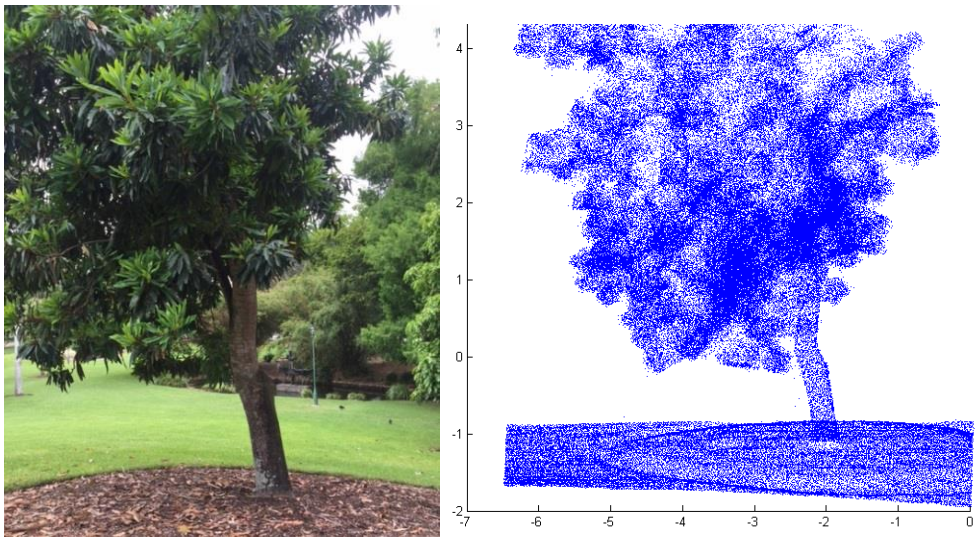

Figure 18 - Image of site 1 located in the botanical gardens (left), point cloud of same image (right).

Site 2 includes a single trunk with minimal leaf material seen in figure 19. This site consists of a palm tree trunk with growth coming from the side at 1.5m, and an average trunk diameter of 30cm. This site represents object that have a constant vertical density for the length of S_z.

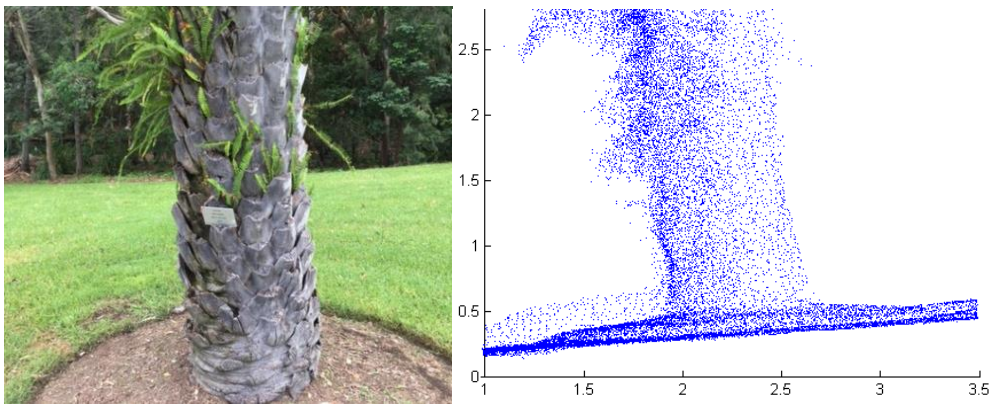

Figure 19 - Image of site 2 located in the botanical gardens (left), point cloud of same image (right).

Site 3 has a fig tree that has sparse under canopy leaf material and long horizontal branches seen in figure 20. This site represents little to no vertical density in S_z.

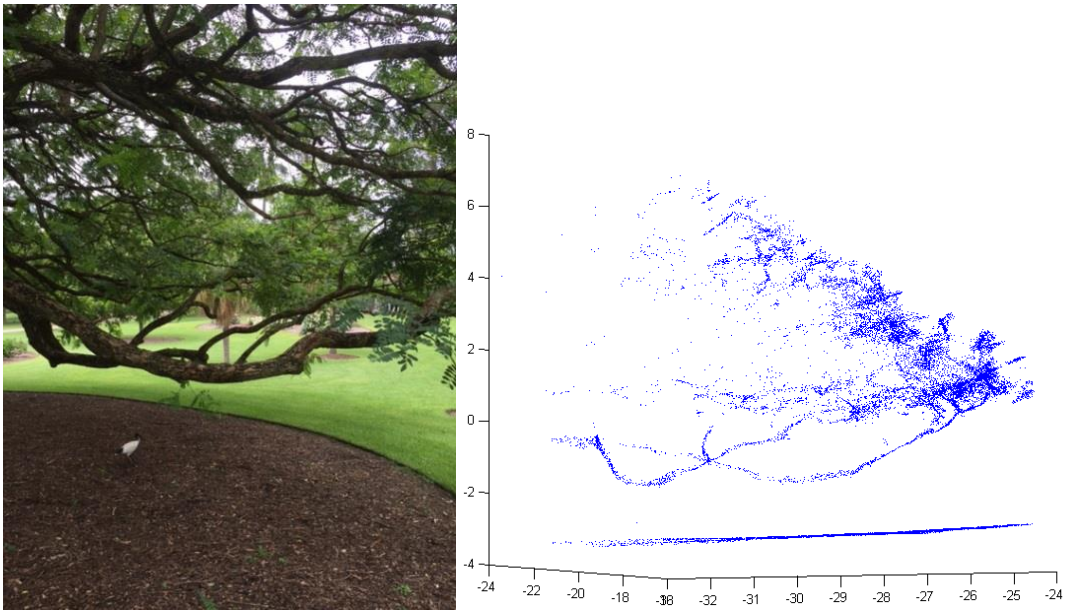

Figure 20- Image of site 3 located in the botanical gardens (left), point cloud of same image (right).

4.1.2 Measurement equipment

Synapse is a USA based software and systems design company. Their product range includes several radio microcontrollers. The Synapse SM700 is structured around a Freescale MC13224V chip transceiver platform. This radio utilises the IEEE 802.15.4 standard at 2.4 GHz. The specifications given by Synapse outline that the SM700 has a maximum transmit power of 100mW with a built-in programmable power output gain from 0dB to +20dB. This unit has been selected to conduct the testing for this experiment. In addition to the output amplifier, a 2.4 GHz 22dBi Omni directional antenna will be used. The SM700 is mass-produced and each unit has its own individual loss characteristics. A paired set can be profiled for the losses in a FSPL test. This paired set can then be use for the object loss testing.

4.1.3 FSPL calibration

The SM700's RSSI feature can be used to sound a channel through sending and receiving packets between two transceivers. The resultant signal strength will indicate path loss through the transmitting hardware, into the air and subsequently through the receiving hardware. By

placing two SM700's at incremental distance from each other and sampling the channel over time, a model of the hardware's profile characteristics can be developed. This model can then be compared to Free Space Path Loss (FSPL) to normalise the results for further testing.

The data set collection method to calibrate the FSPL will be conducted using two nodes; a TX stationary node and a RX semi stationary node. The TX node will be placed in a static position for the tests to represent 0m. The RX node will be moved away from this node in a logarithmic scale along a tape measure. The RX node will be connected to a laptop to record data from both nodes. Each node has an array of on-board functions that allow access to hardware functions. The functions that will be utilised in this test include: Get link quality, scan energy, and transmit information. The Get link quality function returns a positive dB value that represents the negative equivalent of the last received packet to the node the function is called on. The scan energy queries the on-board radio for an ambient energy value for each channel in the 2.4GHz schema. The returned 16 values are the effective noise floor. The final command that is utilised is send data, this command sends a packed of data from one node to the other. This command will send the stationary node's link quality to the base node to be recorded. By utilising an on-board timer and scheduling a packet to be sent every 100ms, we can measure packet loss by counting the incoming packets per second against expected packets per second.

The FSPL calibrations were conducted to establish a profile for the equipment; predicting its accuracy and error at varying distances of transmission against the expected FSPL values. This will be done in an open field. Each node will be mounted at the height of 1.7m from the ground. Placing the transmitted signal above the first Fresnel. From each location 200 samples were taken. This data was then put into SPSS, a statistical program, and filters were used to remove outliers two times the standard deviation, to produce an equation for the samples taken. This equation had a greater rate of loss in comparison to FSPL; in particular the offset was greater seen in figure 21. Both of these factors were expected, as the hardware is not of a scientific standard for absolute measurement. This result could be used in the model to simulate FSPL for this hardware pair.

$$dBm(m) = -5.847 \log_{10} m - 54.324$$

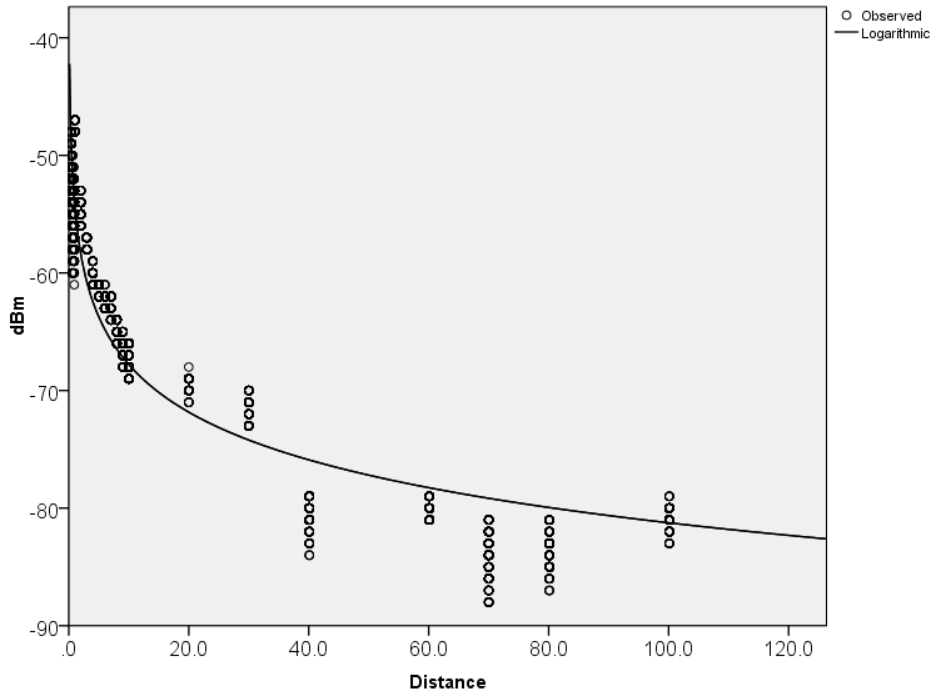

Figure 21 - FSPL calibration curve for channel sounding equipment used in experiment 2 distance in M.

4.2 Method

This experiment aims to capture attenuation of a wireless signal at 2.4 GHz through air, via an intrinsic object using a pair of antennas, denoted as RX and TX. The sampling will begin by isolating features in the S_z map of an individual site. Transects are placed on this map from a common TX point cutting through the features of interest. Several rays using S_z will be simulated for each transect including surrounding angular position, each of these will be analysed looking for points of change in inflection. These are broken down and used to position where RX, TX samples will be taken. The equipment will take 200 samples for each point, rendering a mean value for each position at the height of 1.7m. The mean value is then subtracted from the FSPL calculation using antenna separation distance. The resultant number is the raw signal attenuation between RX and TX as it passes through the object space. This resultant vector of dB/distance will then be analysed with respect to the simulated ray vectors in the results section of this research.

Other considerations that will be taken into account include the surface gradient of ground to the measurement plane with reference to the antenna orientation. Antennas will be maintained at a parallel plane to each other, in order to maximise the results of the Omni Directional antennas. Antennas will be kept above the first Fresnel zone in relation to the ground.

4.2.1 Site 1

This site was chosen to validate the interaction of radio propergation with the a tree trunk and leaf material. Surrounding the tree is cut grass. The tree sits on a medium slope and for this reason the TX point has been placed up hill from the tree. The orentation of the site map is East up. Three transects were positioned on the map emanating from the TX point straight through the bulk of the leaf mass at 90 degrees (East), at an angle through the tree trunk (55 degrees), and finally North (180 degrees) from the TX point to give normalisation to manage calibration.

The 2D slice of site 1, showing S_z at a height of 1m above and below the antenna at 1.7m, is shown in the figure below. A range of values from zero to nine for the respective compressed vertical density column in the z direction with a x y grid spacing of 1cm. This slice has a skewed distribution to the left with a mean of 1.21 and a max of 9. This concertration of single points shows a minimal vertical density for the majority of the leaf portion of the tree. Aditionally, a value of one represents the ground surface seen in the lower quarter of the figure. The postion of the tree trunk is outlined with a black circle. The proposed TX point is maked by the blue circle. Through consideration of this figure, three transects for sampling were taken covering each of the elements, including a FSPL for recalibration. The three transects discussed above are shown in Figure 23 - Site 1 transects. The blue lines represent the path followed by the RF equipment. The green bands show the range of samples that will be used from the S_z map.

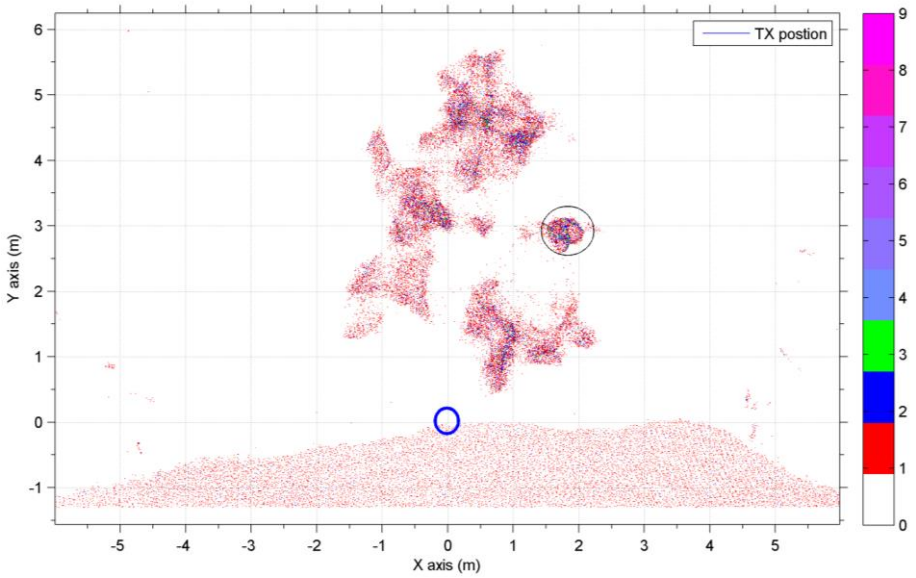

Figure 22 - Site 1 located at the botanical gardens; representing S_z a 2D compression of the vertical point density.

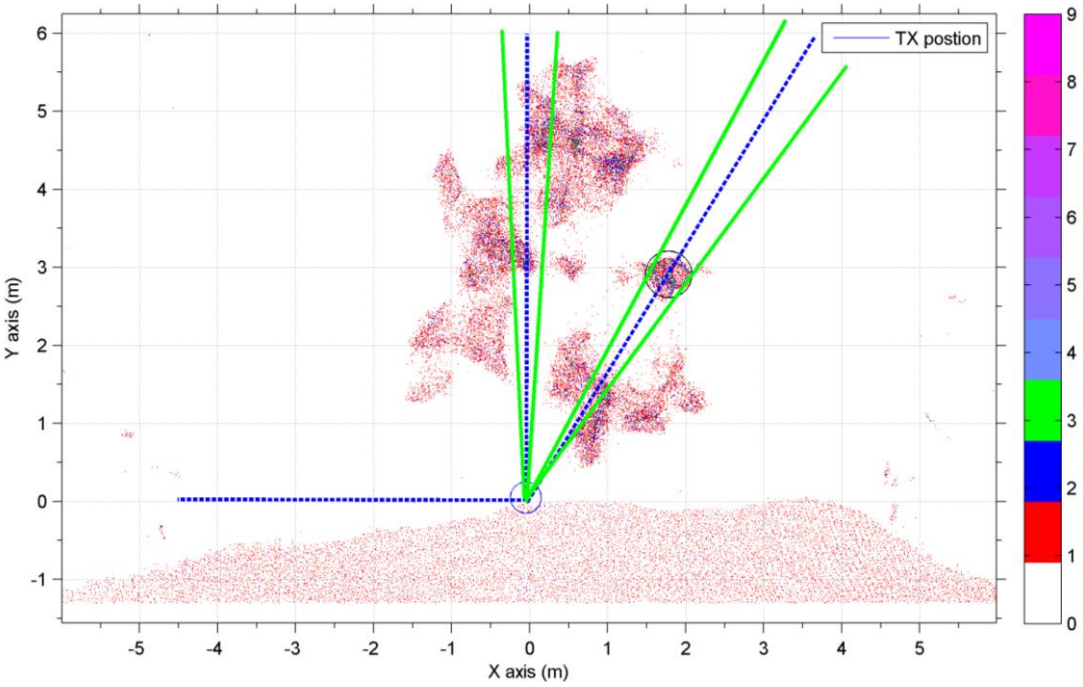

Figure 23 - Site 1 transects emanating from TX poison from right to left, 1-3 in blue dash, green bands representing simulation sample.

Table 2 - Transect angle table for site 1 starting at 0◦ to X rotating counter clockwise.

Transect	Angle from positive x axis
Site 1 transect 1	55◦
Site 1 transect 2	90◦
Site 1 transect 3	180◦

4.2.2 Site 2

Site 2 is located 7m from site 1 to the west. This site was chosen to focus on a single tree trunk with a large diameter. The palm tree that is located here has a rough surface due to the growth of old palm fronds. This can be seen in Figure 24 - Site 2 Additionally, a small amount of new growth palm fronds are present in the upper left portion of the figure. In the lower right portion of the image, a gap can be seen in the point density due to the sampling with the Zebedee; whereby the instruments path was not adequate to capture all angles of the tree. This is likely to happen in many circumstances if site access is restricted or the user sampling does not construct the sample path to encompass all angles of all objects. For this reason, this simulation showed the effects of a case of missing points. This site is orientated South up, the three trances are shown in Figure 25 - , shown in blue heading away from the TX point shown in black at x y (0,0).

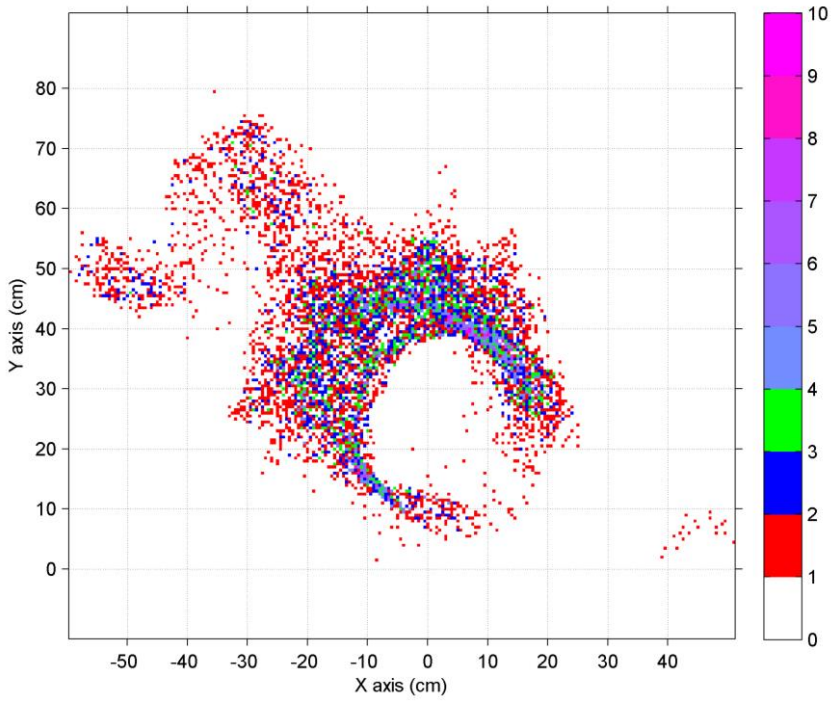

Figure 24 - Site 2 located at the botanical gardens; representing S_z a 2D compression of the vertical point density.

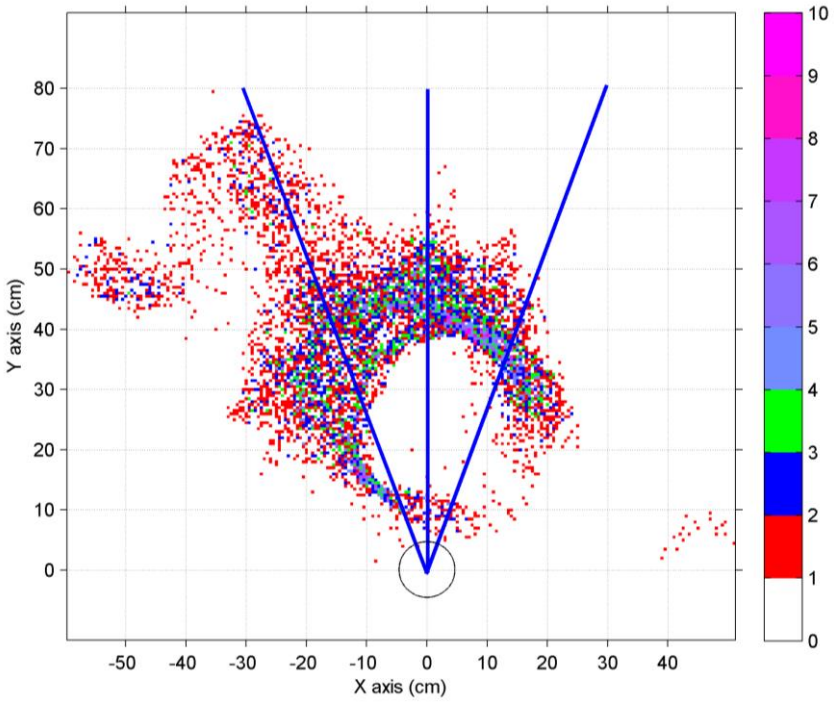

Figure 25 - Site 2 transects emanating from TX poison from left to right, 1-3 in blue lines.

Table 3 - Transect angle table for site 2 starting at 0◦ to x rotating counter clockwise.

Transect	Angle from positive x axis
Site 2 transect 1	141◦
Site 2 transect 2	90◦
Site 2 transect 3	51◦

4.2.3 Site 3

The final site, site 3 was chosen to validate two interactions: the interaction of the signal beneth a canopy of a large tree, and the main interaction with horizontal branches that have a minimal vertical profile. This site is located in the northeast of the botanic sample. Facing north, the site looks into the main tree trunk. The image in Figure 20 (left) shows the site from a westerly aspect. This site has a predominant point value of one seen in figure 26. This indicates that the branche's width is less than 8cm in the vertical plane. The S_z window is the same as before; 2m in height split equally about the antenna height. The three transects emanating from the TX postion for this site have less significance in comparison to the previous sites, as there is little variation in the point density seen in figure 27. To add significance, the transect angles were chosen to isolate height variations in the profile, as the

branch height varys from the trunk in a downward angle. This will show how the height of the object in the profile affects the signal.

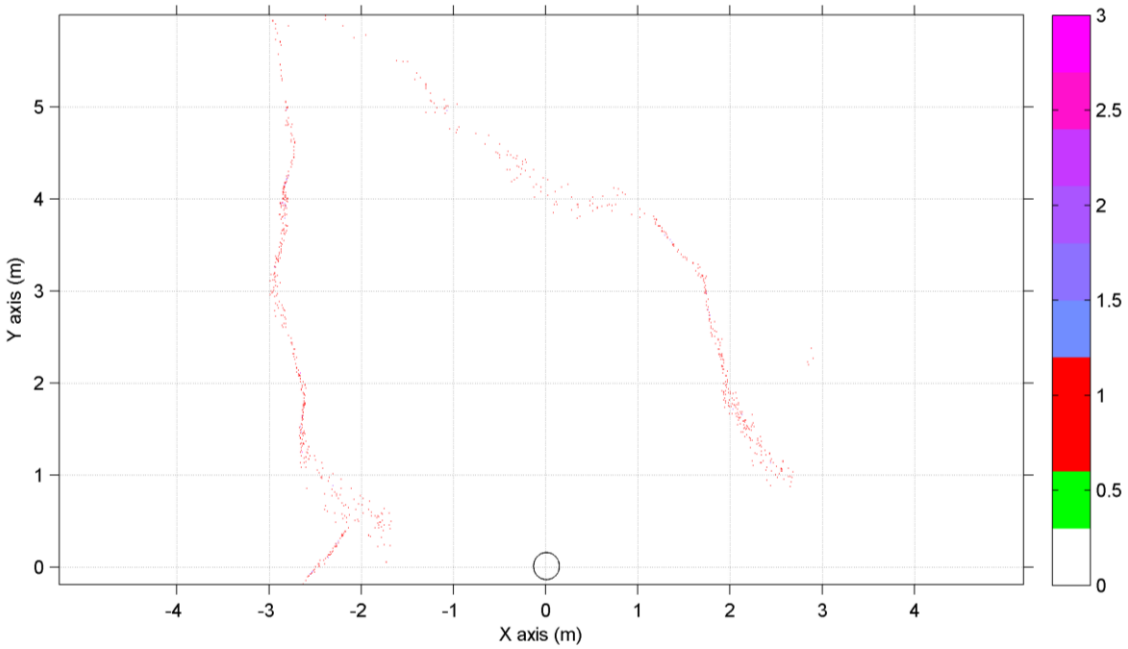

Figure 26 - Site 3 located at the botanical gardens; representing S_z a 2D compression of the vertical point density.

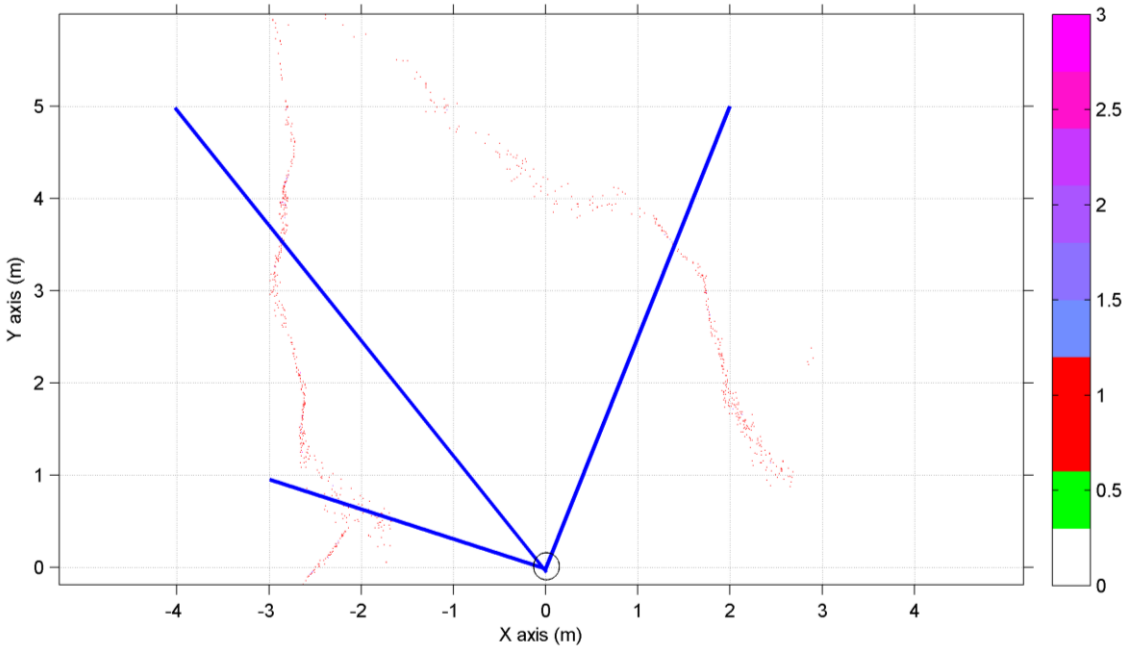

Figure 27 - Site 3 transects emanating from TX poison from left to right, 1-3 in blue lines.

Table 4 - Transect angle table for site 3 starting at 0◦ to x rotating counter clockwise.

Transect	Angle from positive x axis
Site 3 transect 1	161◦
Site 3transect 2	129◦
Site 3 transect 3	68◦

4.3 Experiment 2 summary

In this chapter the measurement equipment for RSSI channel sounding was calibrated using the LOS loss model, calibrating expected results against the actual. Following this RSSI information was captured for three transects across the three sites at the Brisbane botanical gardens. This signal loss data aimed to collect varying profile densities within the LiDaR data, looking at leaf material, a tree trunk, and horizontal branches. The data collected along these transects was then subtracted from the FSPL calibration factor to give pure loss of obstructions along each transect. The next chapter will address how RSSI signal loss is related to the density profile and provide a calibration factor for the model.

Chapter 5

Results & discussion of experiment 1 & 2

This chapter is broken into two sections: 1) investigating a correlation between the data sets, and 2) developing a compensation factor to the simulation of the model in chapter 3. The simulation is re-run for the full site to create a heat map for several TX locations. Each map will then be validated by checking against measurements in locations throughout the site. The signal attenuation due to object obstructions was clearly identified in the second experiment; whereby variations in object density contributed to a signal loss response. The results for each transect are analysed against groups of comparable Ray Traces, in order to account for limitations that were found in the acquisition method of the signal loss transects. It became apparent that the absolute measurement and positioning of the antenna was not achievable in some locations, with leaf material and branches present as obstructions. To compensate for this limitation, broader sampling occurred of the area either side of transects taken from the S_z map. The mean height at the comparable sample location for each transect was taken and used to compare the grouped vectors.

5.1 Comparative analysis

The figures below show a shared linear scaled increase over the length of the two types of vectors. Sites 2 and 3 experienced very low sample points due to constraints of object locations

seen in minimal point representation in Figure 31 to Figure 36. The lack of interpolated points will affect the analysis of signal loss and Ray Trace along the vector. However, all vectors have a final value for each transect in common, and for this reason this was investigated as a possible solution for a scaling coefficient. The table below contains comparative and statistical results of the nine transects. The table compares the average final dB values for the furthest points on the RF transect, the average final value of the selected Ray Traces, the difference between average RF loss, the average Ray Trace final, and the ratio of error between these values. The figures listed below from Figure 28 to Figure 36 are outlined as follows, each site's transect has a RF sample set using experiment two's method. This transect will be presented in red, showing the signal loss in dB with the subtraction of the FSPL element. A dashed line joins the each sample point; this line is a linear interpellation between points. The set of Ray Trace vectors for the surrounding area of the RF transect is represented in blue. Both vectors have the same distance scale in centimetres. The green vectors, along the base of the figure, are the raw density values that are used to calculate the cumulative response in blue.

5.1.1 Site 1 nor-Normalized

Transect 1

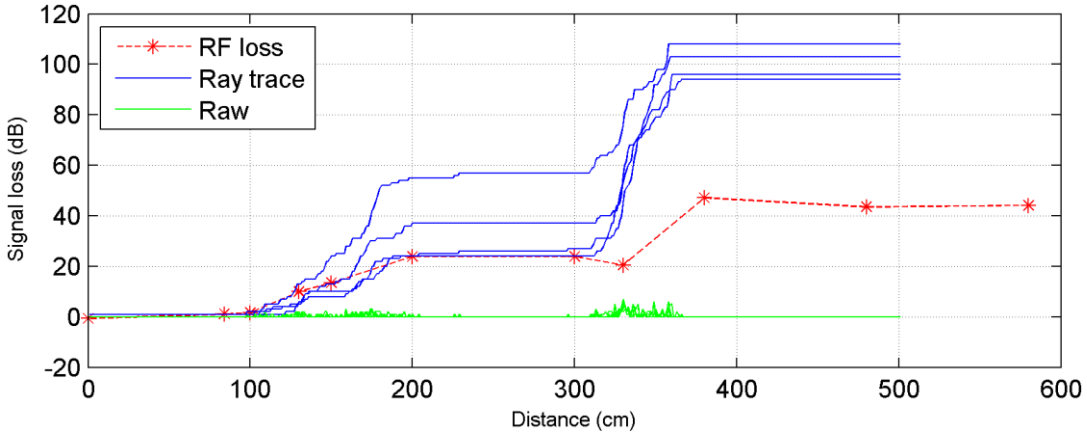

Figure 28 - Site 1 transect 1 botanical gardens; Tree observed RF loss vs simulated Ray Trace.

Transect 2

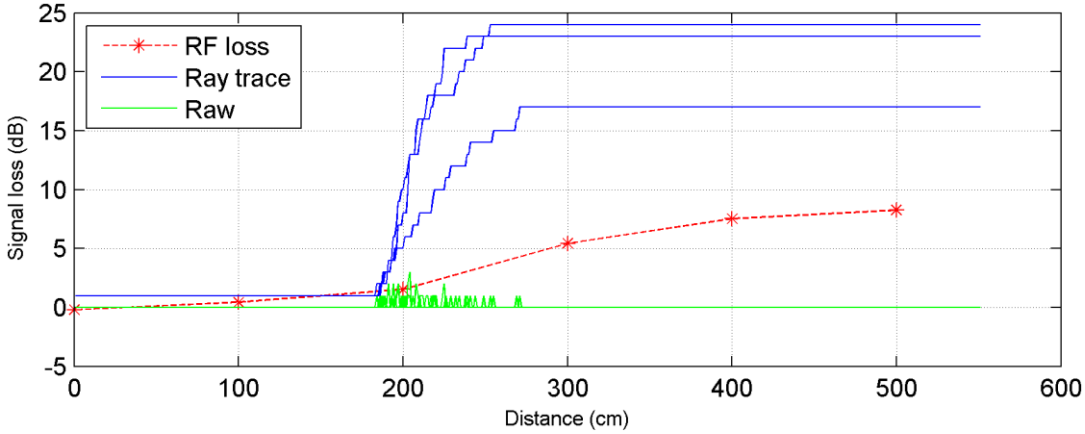

Figure 29- Site 1 transect 2 botanical gardens; Tree observed RF loss vs simulated Ray Trace.

Transect 3

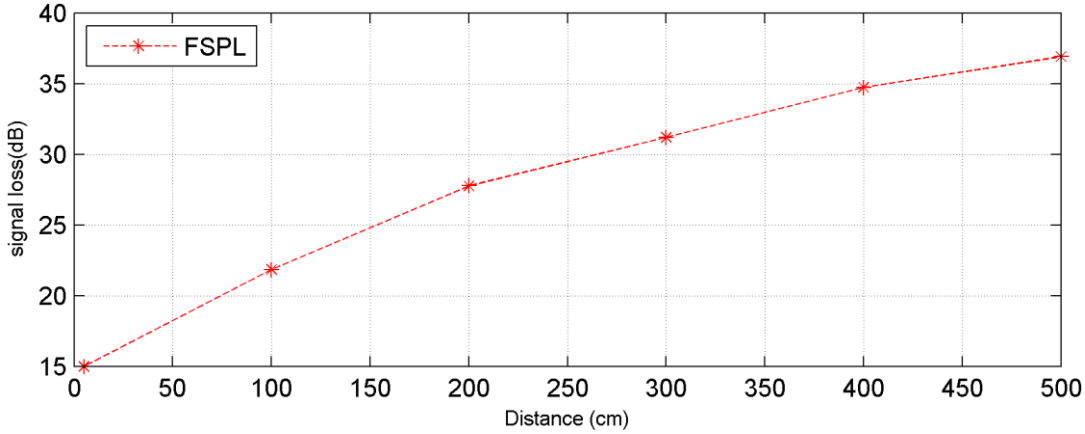

Figure 30- Site 1 transect 3 botanical gardens; Tree (FSPL) for channel sounding equipment.

5.1.2 Site 2 nor-Normalized

Transect 1

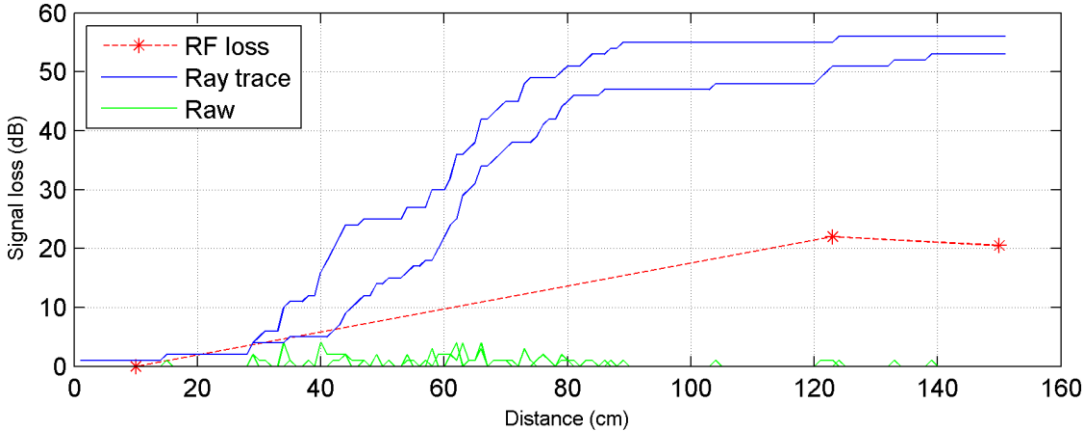

Figure 31 - Site 2 transect 1 botanical gardens; palm observed RF loss vs simulated Ray Trace.

Transect 2

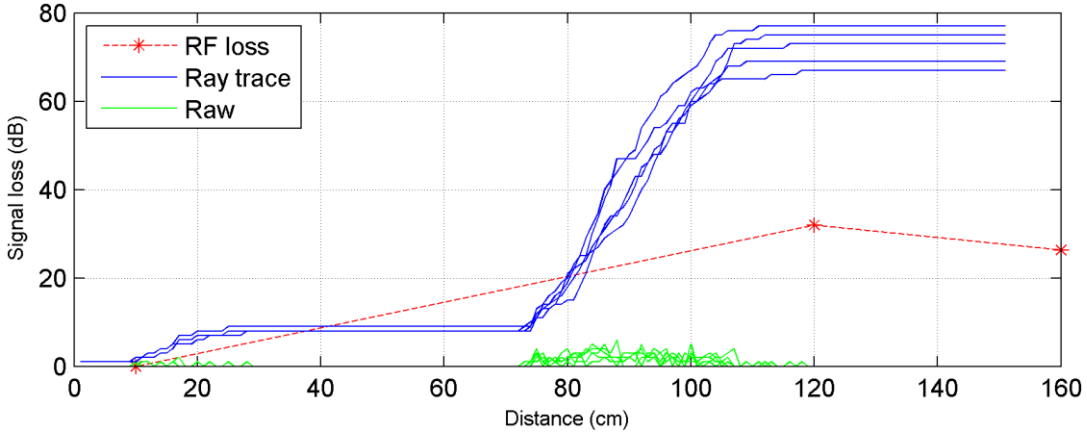

Figure 32 - Site 2 transect 2 botanical gardens; palm observed RF loss vs simulated Ray Trace.

Transect 3

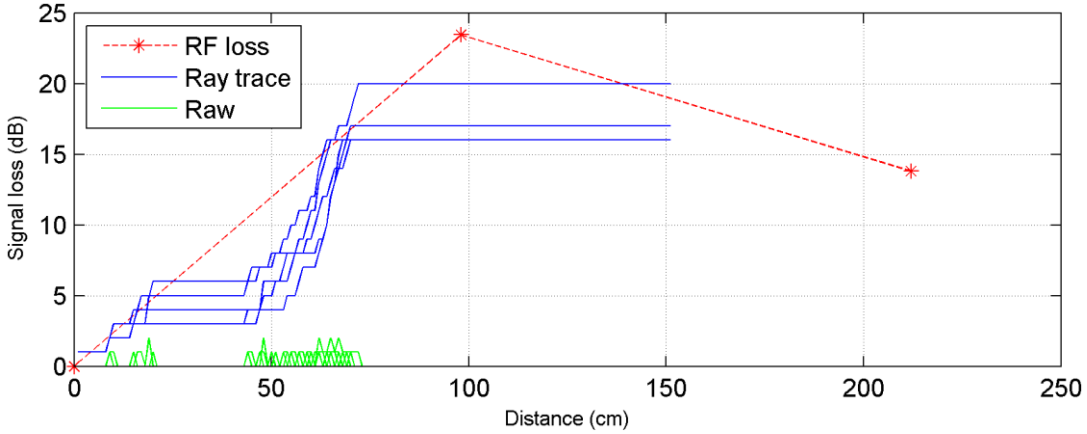

Figure 33 - Site 2 transect 3 botanical gardens; palm observed RF loss vs simulated Ray Trace.

5.1.3 Site 3 nor-Normalized

Transect 1

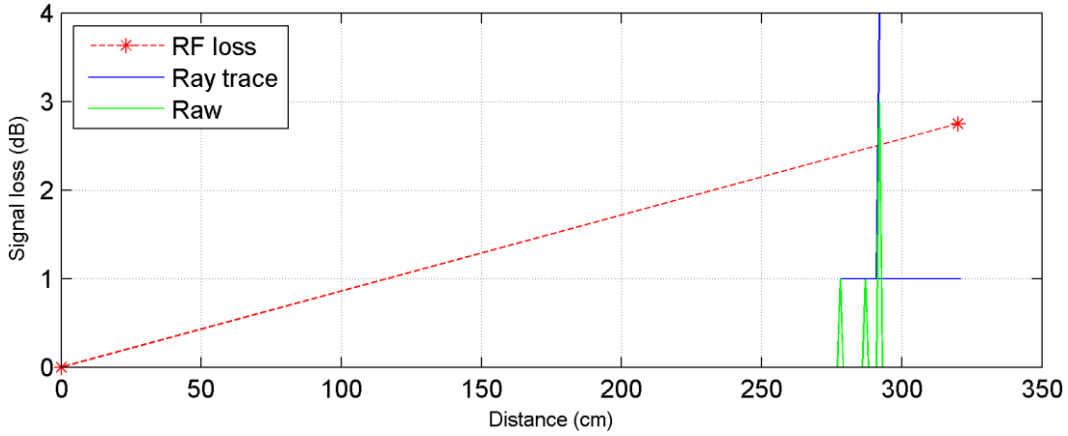

Figure 34 - Site 3 transect 1 botanical gardens; Fig Tree observed RF loss vs simulated Ray Trace.

Transect 2

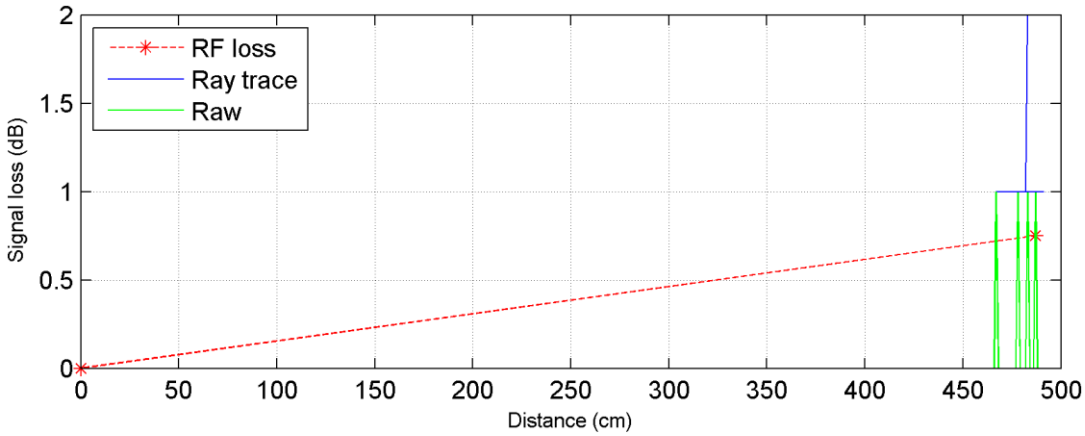

Figure 35 - Site 3 transect 2 botanical gardens; Fig Tree observed RF loss vs simulated Ray Trace.

Transect 3

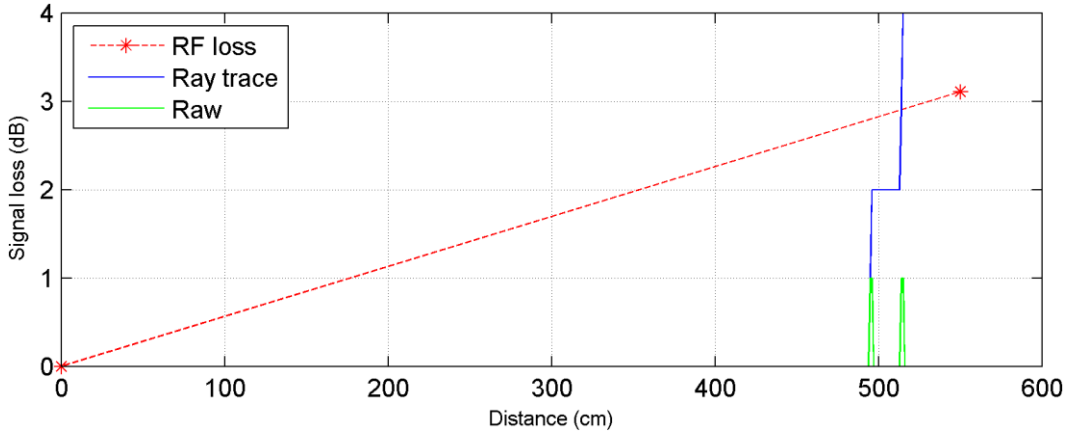

Figure 36 - Site 3 transect 3 botanical gardens; Fig Tree observed RF loss vs simulated Ray Trace.

Table 5 - Measured Results of sites 1-3 from the botanical gardens, comparing RF loss against average Ray Trace.

Location	Average final RF loss dB	Average final Ray	|dB - Ray|	Ratio $_{dB/ray}$
Site 1 Transect 1	45	100.25	55.25	0.449
Site 1 Transect 2	8.2	21 .34	13.14	0.384
Site 2 Transect 1	21.5	54.5	33	0.395
Site 2 Transect 2	29.15	72.2	43.05	0.404
Site 2 Transect 3	17	17	0	1*
Site 3 Transect 1	2.75	3.5	0.75	0.786
Site 3 Transect 2	0.75	2.34	1.59	0.322
Site 3 Transect 3	4.11	5	0.89	0.822*
		Mean	18.46	0.57
		Std Dev (σ)	-	0.19
		Mean corrected*	-	0.457

* excluded values for recalculation.

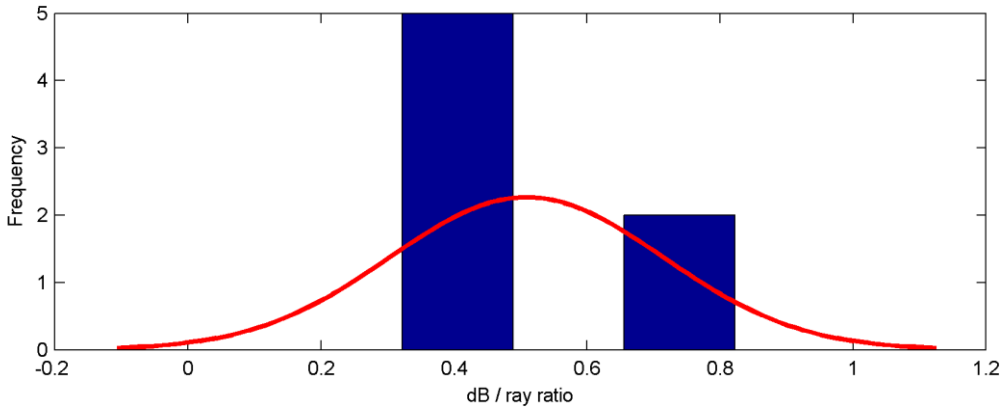

Figure 37 - Normal distribution & histogram of Error ratio for results in Table 5

5.1.4 Comparative results discussion

The comparison table above, of the RF loss final and the Ray Trace average final, shows 100% of the Ray Trace values are larger than the RF loss. The mean value of the error ratio at 57% shows minimal correlation between the current simulation and actual loss. The standard deviation of 0.19 allows for removal of some results that are outside the normal distribution range, figure 37. Sites 2 and 3, transects three and three, respectively, are both 1.5 times the standard deviation from the mean and were removed from further calculations. When excluding these transects, the mean is corrected to 0.457. Additionally, site 2 transect three was outlined as a missing data set, with a significant amount of points missing from the LiDaR sampling**.** Across the sites sampled, a linear scaled correlation is identifiable as the expected follows the path of the simulated. This suggests that scaling the Ray Trace vectors with a component to calibrate the model will correct the simulations results.

The data collected at site 3 exhibits a poor error ratio for all transects compared to sites 1 and 2. This was attributed to the quantisation level of the Ray Trace vector method. The RF signal values for these sites are less than 5dB. Therefore, equally as many points for the ray are available, leaving a large error ratio while having a minimal subtraction difference. For this reason, results for the error ratio for site 3 will not be taken into account as a significant result. Additionally, these results are expected due to a low density number for S_z for this site. The corrected mean error value of 0.457 was substituted as a scaling factor to analyse how the scaling coefficient would adjust the Ray Trace vector's vs observed RF loss.

5.1.5 Site 1 adjusted comparison

Transect 1

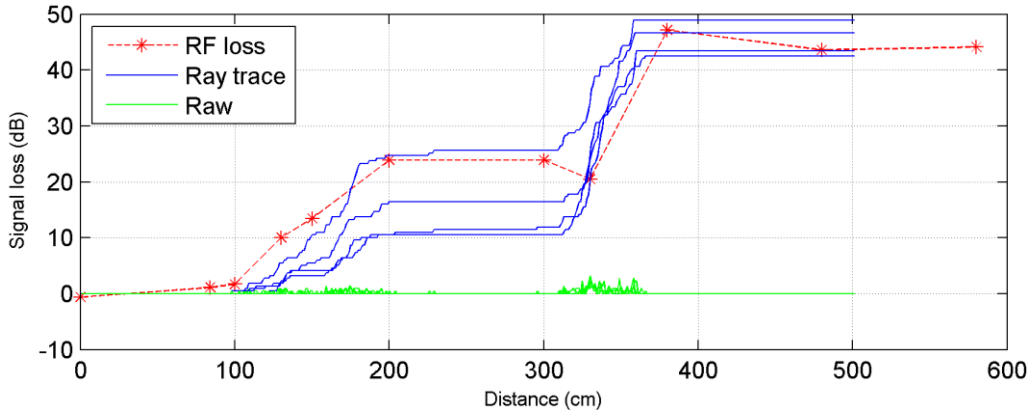

Figure 38 - Site 1 Transect 1 botanical gardens; Tree observed RF loss vs simulated Ray Trace scaled by 0.457.

Transect 2

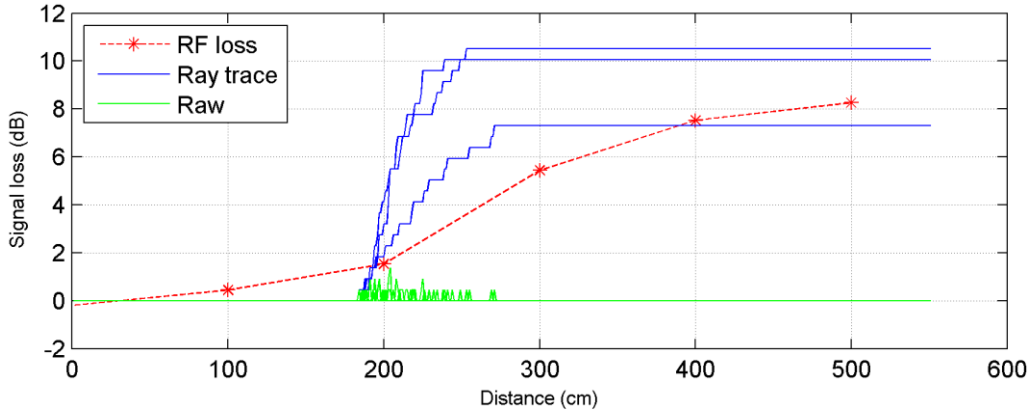

Figure 39 - Site 1 Transect 2 botanical gardens; Tree observed RF loss vs simulated Ray Trace scaled by 0.457.

5.1.6 Site 2 adjusted comparison

Transect 1

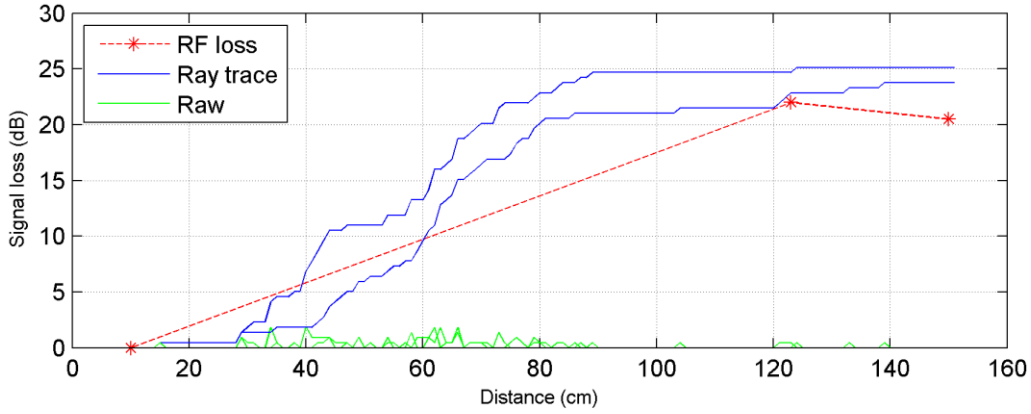

Figure 40 - Site 2 Transect 1 botanical gardens; palm Tree observed RF loss vs simulated Ray Trace scaled by 0.457.

Transect 2

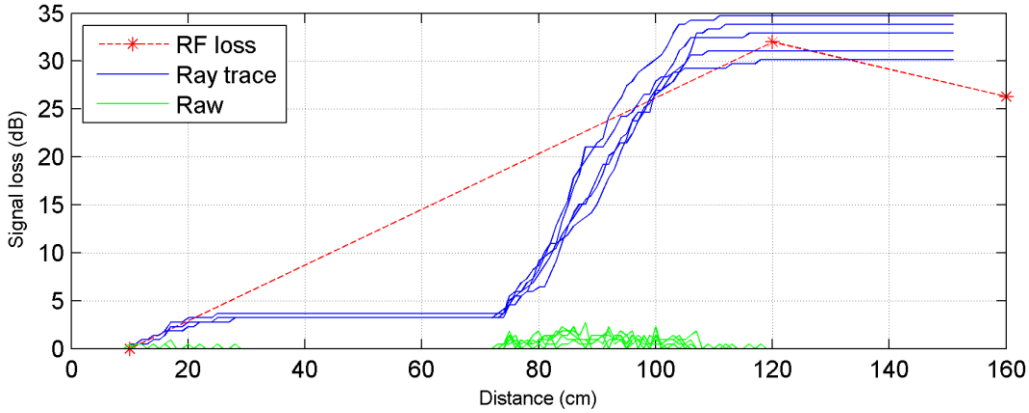

Figure 41 - Site 2 Transect 2 botanical gardens; Tree observed RF loss vs simulated Ray Trace scaled by 0.457.

Transect 3

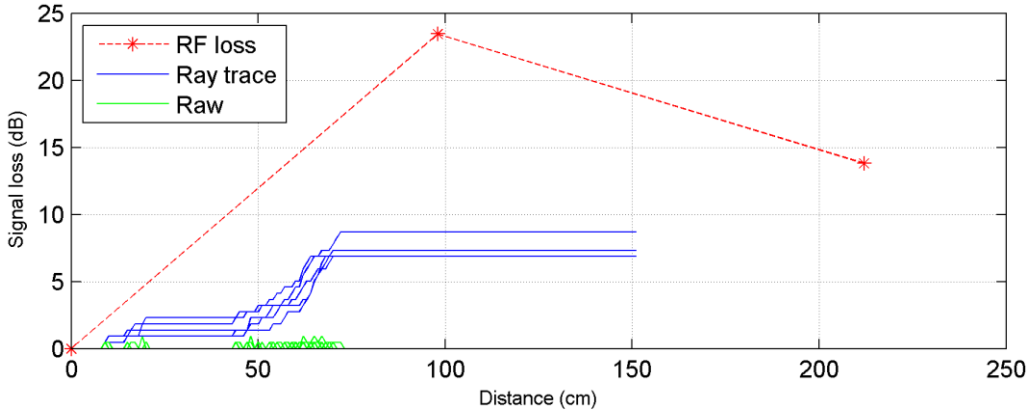

Figure 42 - Site 2 Transect 3 botanical gardens; Tree observed RF loss vs simulated Ray Trace scaled by 0.457.

5.1.7 Site 3 adjusted comparison

Transect 1

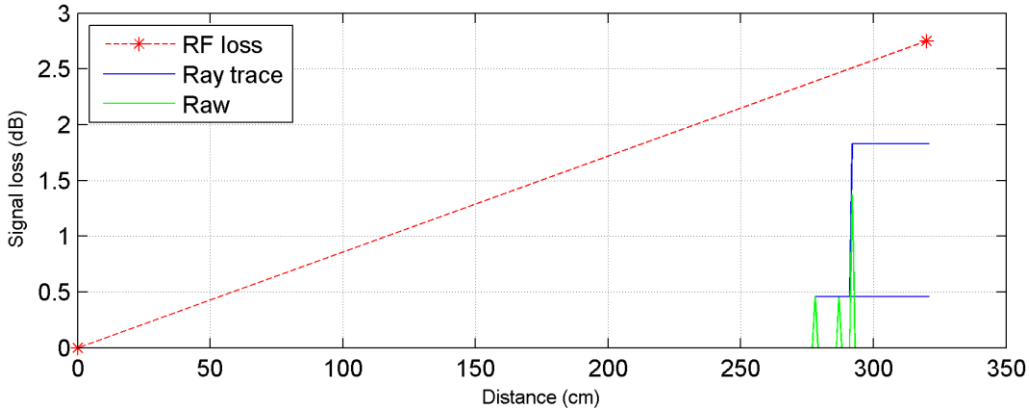

Figure 43 - Site 3 Transect 1 botanical gardens; Fig Tree observed RF loss vs simulated Ray Trace scaled by 0.457.

Transect 2

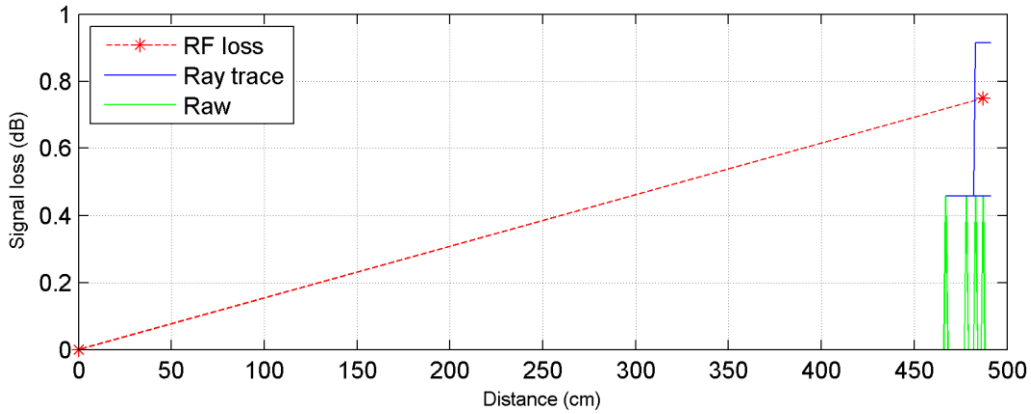

Figure 44 - Site 3 Transect 2 botanical gardens; Fig Tree observed RF loss vs simulated Ray Trace scaled by 0.457.

Transect 3

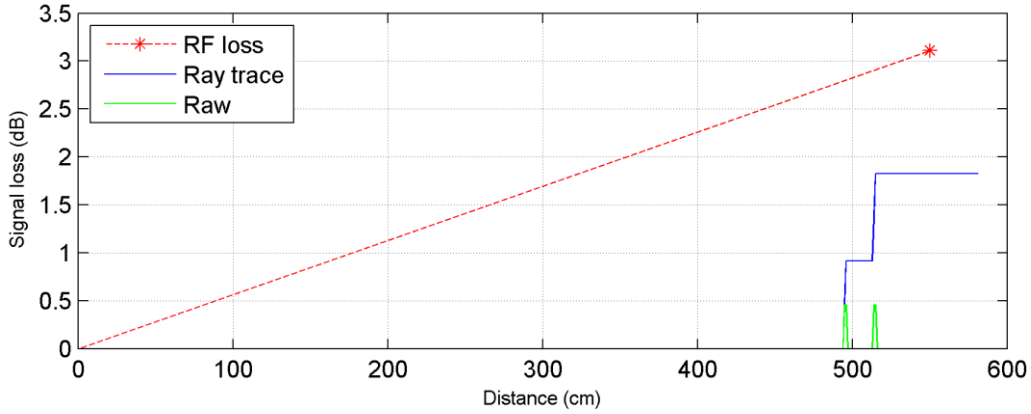

Figure 45 - Site 3 Transect 3 botanical gardens; Fig Tree observed RF loss vs simulated Ray Trace scaled by 0.457.

Table 6 - Measured Results of sites 1-3 from the botanical gardens, comparing RF loss against average Ray Trace scaled by 0.457.

Location	Average final dB	Average final Ray	|dB - Ray|	Ratio $_{dB/ray}$
Site 1 Transect 1	45	45.36	0.36	0.99
Site 1 Transect 2	8.2	9.3	1.1	0.88
Site 2 Transect 1	21.5	24.45	2.95	0.88
Site 2 Transect 2	29.15	32.5	3.35	0.90
Site 2 Transect 3	-	-	-	-
Site 3 Transect 1	2.75	1.14	1.61	2.4*
Site 3 Transect 2	0.75	0.61	0.14	1.2*
Site 3 Transect 3	4.11	1.83	2.28	2.25*
		Mean	1.68	0.91
		Std Dev (σ)	1.148	0.045
		Max error (dB)	3.35	-
		Min error (dB)	0.36	-

* excluded values for recalculation.

5.1.8 Adjusted comparative results discussion

The results from the use of the scaling coefficient above had a significant improvement on the overall reduction in the disparity of final values. Specifically, reducing the mean difference from 18.46dB to 1.68dB, and decreasing the maximum difference to 3dB and a minimum difference to 0.36dB. The ratio error also became smaller, with an ideal value of 1 as to 100%. Furthermore, the mean error was lowered to 91% with a standard deviation of 4.5%, when excluding site 3 results.

5.2 Model Simulation

The mean value of 0.457 used in scaling the Ray Trace algorithm was used to generate a heat map for each site. These simulations were prior to the addition of the FSPL element to show the exclusive loss due to objects within the transition line. The matrix D_{Rt} was subtracted directly from the FSPL image of the same size generated using the same TX position. A shadowing like effect extended beyond the objects due to the accumulation of points along the ray with a cumulative response.

5.2.1 Site 1 RF loss heat map

The image in figure 46 clearly shows the three areas of main interest from site 1. These areas are clearly identifiable with the tree and leaf material extending from TX position to the right corner, with a range of values from less than 10dB to 40dB. The leaf material of the second transect extends from the TX position directly up along the y axis. This region has values ranging from less than 10dB to above 50dB. The second transect extends from the TX point to the top right hand corner. The FSPL ray extends to the left of the image along the horizontal axis at a y value of 600cm.

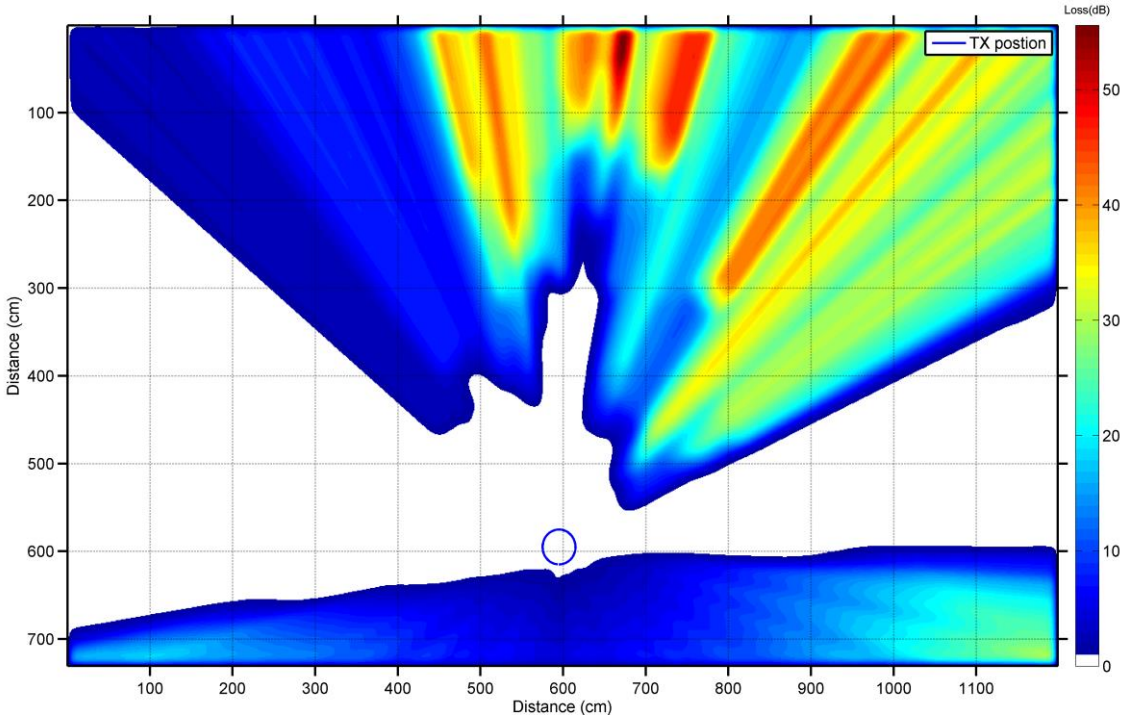

Figure 46 - Site 1 Ray Trace heat map botanical gardens, D_{RT} signal loss

5.2.2 Site 2 RF loss heat map

The second site's heat map shows a deficit in the lower right hand portion of the image. This is due to the missing points outlined previously from gaps in the LiDaR acquisition. The backside of the tree is consistent and uniform with the results. The left portion of the tree experiences a very high loss due to the tree trunk and additional growth of fern frons that are present. The first transect for this site is projected through this point and has a higher error ratio in comparison to the second transect through the centre on the palm. This denotes that the model experiences a higher degree of error at the edges of a surface in comparison to vectors that pass through perpendicular to the object.

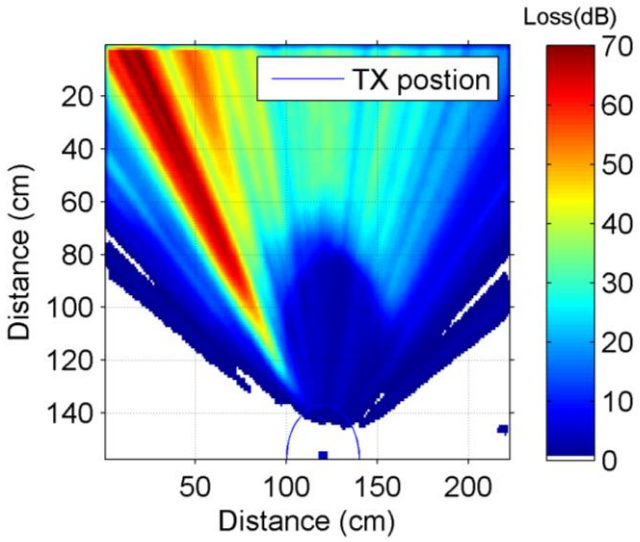

Figure 47- Site 2 Ray Trace heat map botanical gardens, D_{RT} signal loss

5.2.3 Site 3 RF loss heat map

The final site demonstrates how a horizontal object with a low density profile has a low impact signal loss factor. This site of two branches extending predominately in a horizontal direction at a height of 1.5 m from the ground only exhibits a loss of 0.5 to 2dB in the heat map. Measurements from the RF testing found losses of 0.75 to 4.11dB. These measurements occur at distances up to 6m, where the 3.41dB different in reading could be partially affected by antenna position and measurement with FSPL subtraction error. FSPL Error is calculated at 0.2dB per 10cm between the ranges of 1m to 10m

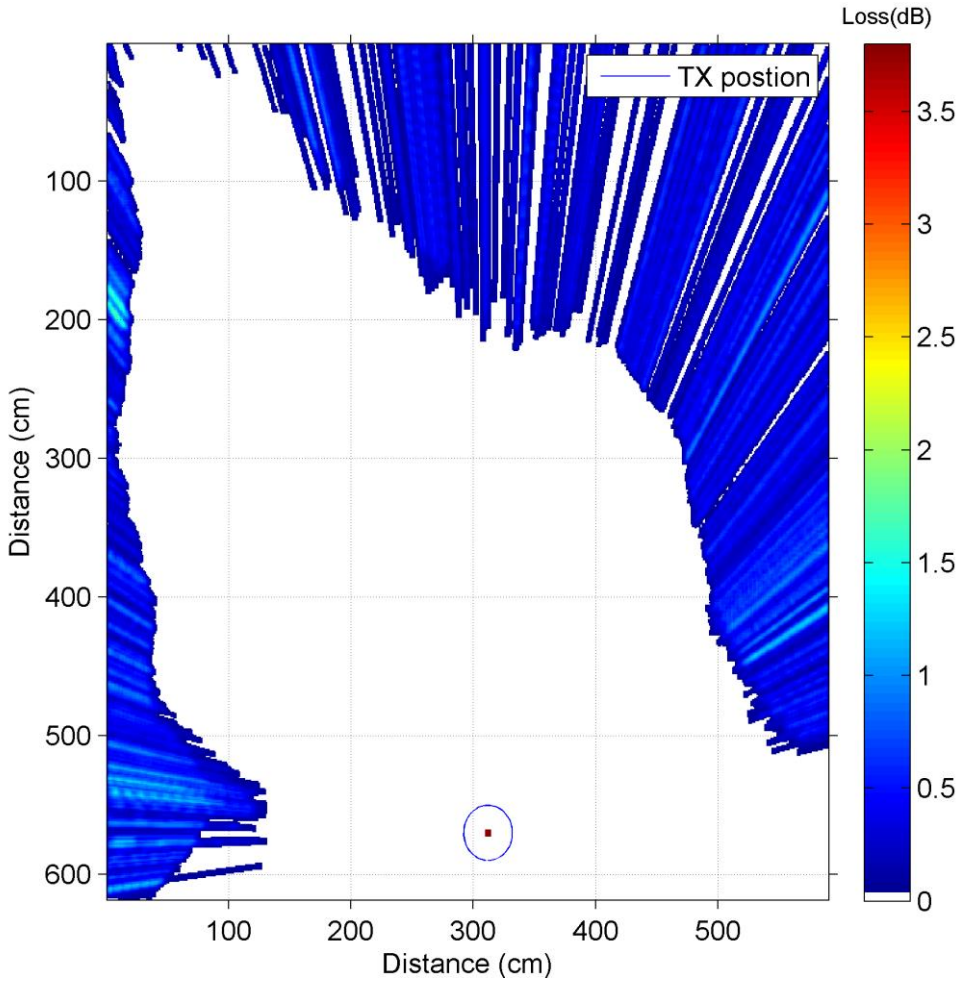

Figure 48- Site 3 Ray Trace heat map botanical gardens, D_{RT} signal loss

5.2.4 Botanical site RF loss with FSPL heat map

The full botanical site simulation incorporates RF loss from simulations with FSPL at a TX position equitant to the first site located at the botanical gardens. This is shown in Figure 49 – Botanic gardens site, full simulation. The simulation shows 1000m^2 of the botanical gardens with a colour bar graduation from +10dB to -120dB. A cut off of -95dB is indicated in this colour bar with the distinct change from brown graduating to black. The lower central section between 2000-6000 x and 6000-9000 y shows the loss due to the gradual slope of the hill behind the transmitter. This area of the heat map is not considered accurate, as it has not been tested for in the calibration. This simulation used the following equation with k representing the scaling constant for the matrix $D_{RT.}$

$$R_{dB} = M_{FSPL} + D_{RT} * k$$

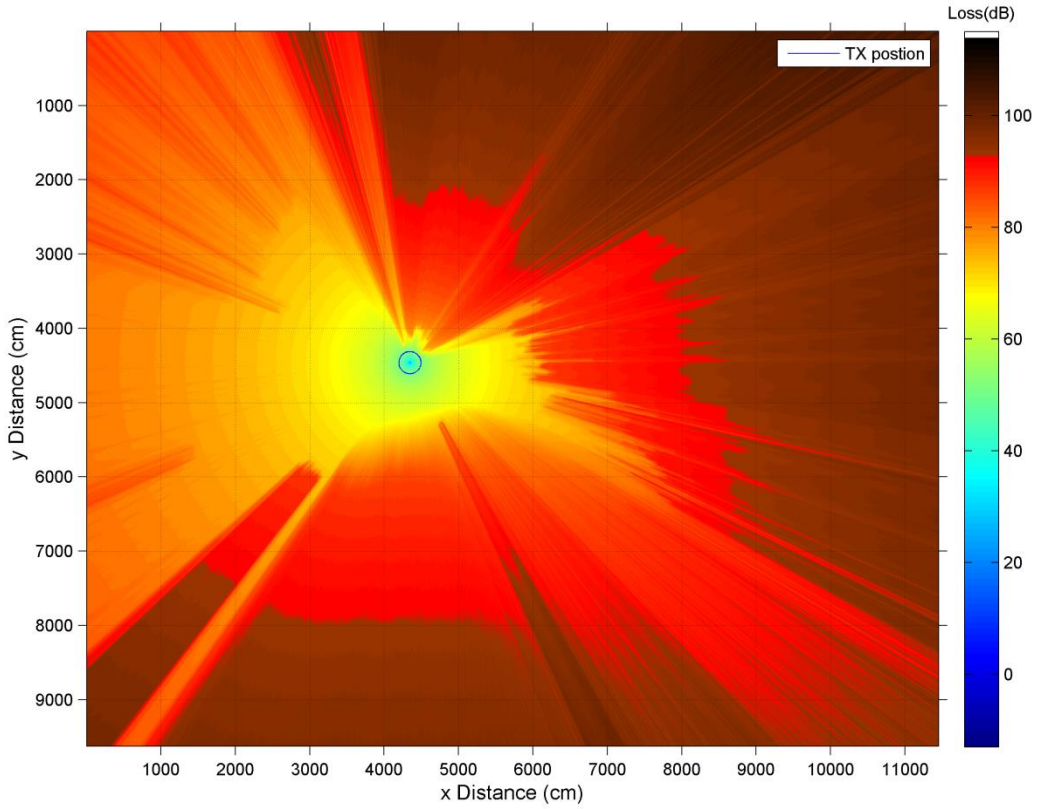

Figure 49 – Botanic gardens site, full simulation $R_{dB} = M_{FSPL} + D_{RT} * k$.

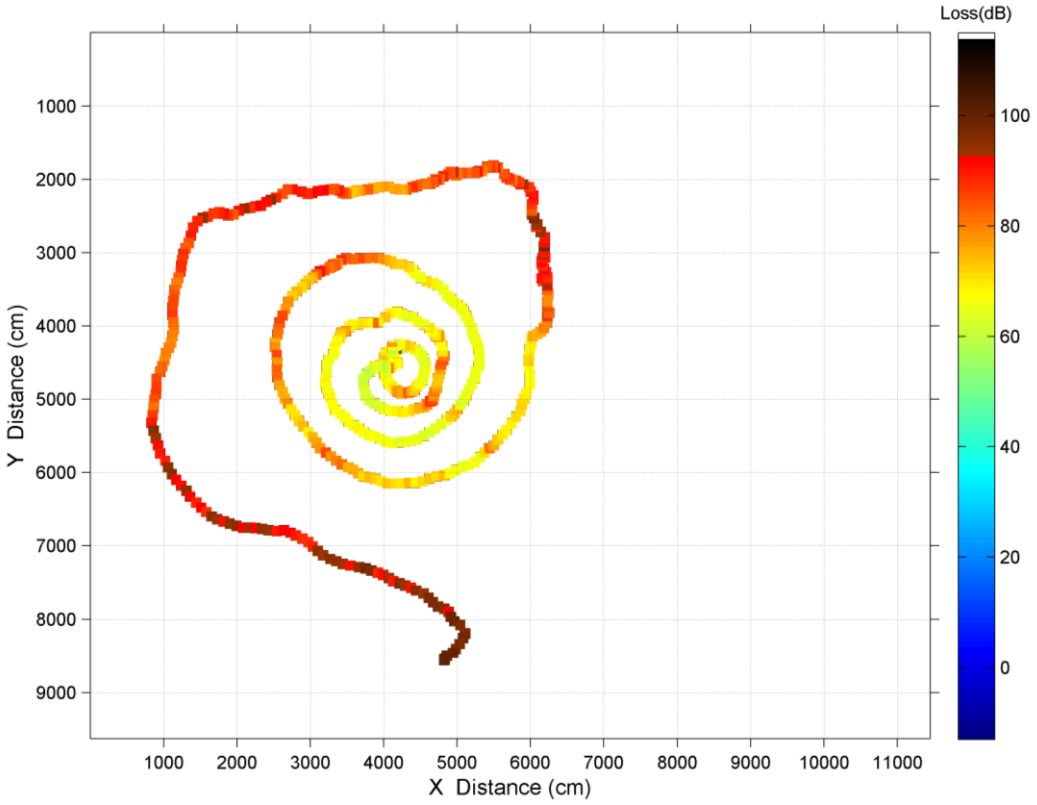

Figure 50 - Observed RF signal loss for botanical site using a set of RX and TX nodes used in the second experiment.

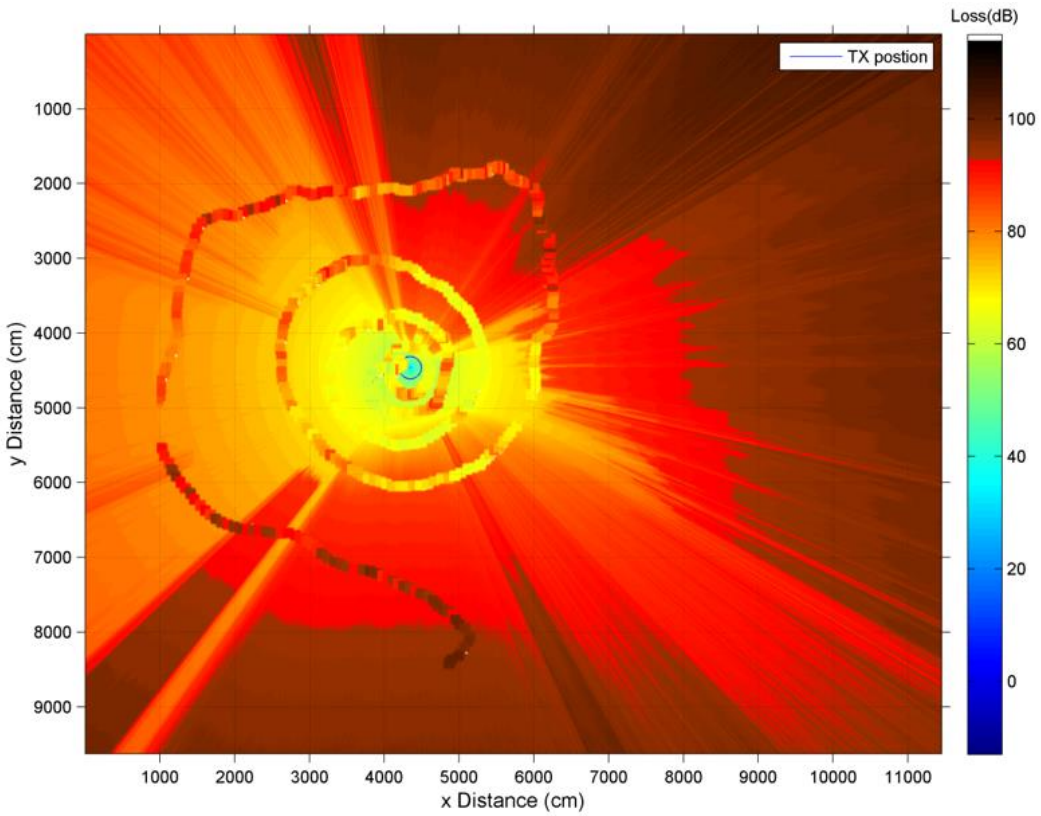

Figure 51 – Observed RF signal loss overlayed on simulated signal loss

5.2.5 Simulation confirmation

The observations in Figure 50 are GPS spaced RSSI measurements taken using a set of RX and TX nodes. The TX node was positioned at the same point of simulation as Figure 49, while the RX node moved in a concentric fashion away from the central location. The GPS measurements paired with RSSI measurements were recoded to build a moving transect. This method allowed the simulated heat map to align with measured RSSI data, shown in Figure 51. The measured RSSI data in Figure 50 had a 70 pixel averaging filter applied to it to increase the size of each pixel for the purpose of making the measurements visible.

The two figures, Figure 49 and Figure 50, share many similar features. Elements that are present in the simulation that caused a shadowing like effect on the signal can also be seen in the measured RSSI data. GPS accuracy of two meters for this test must be considered when comparing the values of RSSI to the simulation results. The overall simulation dimensions of 10m X 12m constitutes to a 20% accuracy variation in the GPS position. Due to this error each

data set cannot be directly correlated with specific points of the simulation. It was noted that the general loss characteristics with respect to locality were similar.

5.3 Design strategies

The resultant heat maps produced by this method are intended to be used with the discretion that an increase to LOS conditions will optimise inter node communications. Characteristics associated with hardware limits and SNR should be considered additionally to the predicted signal loss. Where this model aims to estimate signal there is a degree of error and this should be considered when calculating maximum loss between nodes.

5.4 Result and discussion summary

This chapter addresses the comparison between simulated and measured RSSI transects at the Brisbane city botanic gardens. Showing the initial results alongside each other in a distance vs loss figure. Following this an adjustment factor was applied to the simulate RSSI. Using a scaling constant the ray trace for each transect. The resultant comparison used first order statistics to find a maximum error across the sites of 3.5dB. After completing the calibration phase this factor was applied to each site's simulations. A final simulation of a new location within the Brisbane City botanic gardens was conducted and compared with a GPS referenced set of RSSI measurements. This comparison highlighted consistent signal loss comparisons.

Chapter 6

Conclusion

The of RF signal loss through complex wireless environments is conventionally difficult to predict prior to deployment without the use of complex and expensive software simulations. Conventional signal loss formulas such as LOS and Empirical direct path models do not account for small variations in environmental objects. Making pre deployment positioning strategies difficult to estimate. This research found evidence to support a relationship between RF signal loss and a vertical density estimation of objects within a LiDaR point set. This resultant relationship was developed into a 2D simulation tool that predicts signal loss using a spatial heat map. Using a method of ray tracing, signal loss emanating in an outward direction is created until a maximum value is reached. Transmission points can be simulated from any given point within the LiDaR point set. Along with a SNR specification, nodes can be spaced across a network relative to each other bound by overlapping link quality estimations.

This process would cut out additional physical channel resampling, therefore reducing the overall time and cost of planning a network. Using this method in the design phase with the aim to position nodes in minimal signal loss areas would facilitate improvements to such techniques as transmission power reduction. Additionally increasing the network power efficiency and life span in battery reliant nodes.

6.1 Limitations

This research has found significant relationships existing between vertical density profile and signal loss propagated along the horizontal plane. Despite this, several limitations were found within the simulations that cause incorrect results. The model is suitable for producing an increased loss factor when the angle of the projected Ray Trace approaches parallel to a surface (i.e. the side of a tree trunk). However, the model does not compensate for variations in ground height. If the rays intercept the ground they are treated like any surface and having a very low vertical density given from the gradient of the slope. Therefore, invalid readings may be generated when interacting with such surfaces. Additionally, sloping hills can induce a multi-path or reflected path, fading element that the model does not calculate. This could be implemented by locating the ground plane through the use of a Digital Elevation Model (DEM) and incorporating this data into the calculations. In this case a 2 ray model would be used instead of a FSPL model.

6.2 Further studies

This simulation technique can be further developed through calibrating it to an airborne LiDaR system for large scale mapping simulation. Future research should attempt to calibrate the model to be used in conjunction with other radio frequencies and device types. Implementation of this method might be better suited to an infield tool that uses a stationary LiDaR system at the position of the RF node and takes into account only the surface profile from that position. Such method would eliminate problems with the surfaces converging on parallel to the Ray Traced.

This system could be adapted to be placed on a moving RN node that would be aware of its surroundings and be able to calculate signal loss to other nodes based on its position, primarily useful in dynamic moving environments.

Appendix A

Light Profile Experiment

Lighting profile for solar energy harvesting

The lighting profile beneath the SERF canopy can be severely affected throughout the day. The energy harvesting characteristics for each node are directly affected through this change in light intensity, due to the nature of the solar cell having a short circuit current proportionality to the available sunlight [40]. To accommodate for this reduction in light through the shading of the taller trees, a lighting profile was generated using a light survey. This was conducted to measure the peek available period throughout the day in LUX (measure of luminance). This survey was conducted at several node locations to give a wide variation of the light available below the canopy.

To understand how this data can be applied, the relationship of LUX to power conversion needed to be understood. The standard test condition (STC) used to test solar panel output power is $1kW/m^2$. This corresponds to the air mass (AM) 1.5 standard describing spectral intensity produced by the sun at 42.8^0 South, latitude. The spectral distribution of AM1.5 spans from 300nm to 2400nm. This does not directly correspond to the spectral output from a LUX meter 380nm to 780nm and the solar cell usable iridescence ranges of 300nm to1200nm [41].

Table 7 - Spectral distribution comparison of source and receivers

Source / receiver	Spectrum
Sun at AM 1.5	300-2400nm
LUX meter	380-780nm
Solar cell	300–1200nm

According to the conversion of irradiance E(W/m^2) to luminance E_v(LUX) given by;

$$E_v = K_m \int_0^\infty E_\lambda(\lambda) Y(\lambda) \mathrm{d}\lambda$$

The product of irradiance $E_\lambda(\lambda)$ luminosity factor $Y(\lambda)$ integrated through the K_m with a coefficient of maximum spectral efficiency, 688lm/W at 555nm. Using this formula and the irradiance for AM 1.5 (1000W/m^2) the return of this function is 100kLUX. Therefore 1kW/m^2 = 100kLUX [41]. This proportionality reflects the previously stated proportionality of current to available sunlight. A. Virtuani et al, found with a reduction in LUX intensity there was a decrease in solar cell efficiency.

Design

Obtaining the LUX survey data will be done through the use of six Hobo light and temperature sensor placed at six sites over the property. As the sensor sites that the nodes will be ultimately placed at are critical, these will be the chosen sites for placement of these sensors. Using a satellite map that has overlayed sensor locations, a group of three sites that are in an open type field location and three sites that are in a closed canopy location were chosen to give a control for comparison. These same sites were used in the latter experiment to maintain consistency throughout the project.

Methodology

The Hobo sensors have a light dependant resistor (LDR) that measure LUX. This sensor must be placed in an orientation that is similar to that of the solar cell. In the southern hemisphere it is recommended that a solar panel should be mounted at an average angle of 25° in a northerly direction. This is the most optimum position for a solar panel to receive a full day's sunlight as the sun passes across the sky from east to west. Therefore, this placement of the Hobo will give the equivalent light exposure throughout the day including any shading that is produced by the canopy.

Table 8 - Sample sites for lighting profile

Site	Serial number	Latitude	Longitude
1	10511474	-27.391366°	152.874982°
2	10511473	-27.390990°	152.875434°
3	10511472	-27.390762°	152.875629°
4	10511471	-27.391904°	152.877187°
5	10511470	-27.391306°	152.877546°
6	10504470	-27.390575°	152.877965°

Appendix B

Design & construction plan

The literature review highlights research on power savings in a WSN has two main approaches. The first approach is to achieve power savings locally on the networks nodes. The physical nodes power saving can be made with algorithms that send the microcontroller and sensors to sleep when idle or driven by external triggers. This type of power saving is ultimately scalable for all hardware of the same type and architecture. Local power savings, however, are not universal to all applications whereby sampling methods change due to the requirements of a node. Therefore, this technique will have isolated outcomes rendering it to a site specific implementation. The second but main focus of the research is to highlight network biased energy savings. This research commonly has an overall focus on achieving the most reliable and low cost method to send a message from the source node to a gateway or sink. This is achieved through several sub-methods that can compound to increase efficacy, including; routing methods, transmission power control, network planning, channel hopping, and rate adaption. These methods rely on the transmitted message received with minimal retries.

Hardware

Low power WSNs primarily use the IEEE 802.15.4 standard to govern the communications between nodes. This is uniform between most platforms in this category. The proposed testing

hardware by Synapse also utilises this standard. This standard outlines methods of testing and ranging as a part of standard. Synapse implementation of the standard does not include user access to all of these features. This limitation restricts ranging techniques to RSSI and measured distance.

The IEEE standard provides a definition for the physical layer (PHY) and median access control (MAC), with specifications for low-data-rate wireless connectivity [42], limited to layers below the upper layers shown in the figure 52. The upper layer consists of a network stack configuration. This holds the message routing and an application layer that provides the function of the device. The standard used in this research is a pre-existing part of the hardware and cannot be modified due to its inaccessibility. However, it will need to be referenced to understand any restrictions that it might have upon the protocol associated with the CSMA-CA algorithm that is used in 802.15.4.

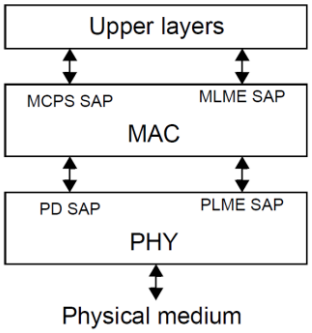

Figure 52 - LR-WPAN device architecture [42].

Design & implementation

The design methodology will consider all of the constraining factors and develop a system that can maximise power efficiency. The Synapse module comes as a PCB composite with surface mount pads. To operate it requires a regulated power supply and breakout access to the I/O. This will be done through the production of a PCB board. Additionally, energy harvesting techniques will be used to combine the Synapse microcontroller with a power supply, breakout board and water proof enclosure for the system.

Hardware research plan (6 weeks)

Hardware research for this system was driven by the sensory devices connected to the final design. This focuses on facilitating the three protocols used in the soil moisture sensors for SERF.

PCB prototype plan (4 weeks)

The systems' PCB board was designed in Cadsoft Eagle and consisted of two prototype stages. The first prototype was produced using QUT's PCB facilities. This machine is only able to cut single sided boards. This constrained the way in which the first board was designed. The second prototype consisted of fixing and adding any additional items overlooked in the first stage. The second prototype also included initial stages of readying the PCB board for printing in a small run prototype factory to reduce the size and increase the board quality.

Hardware testing (9 weeks)

Hardware testing encompassed several phases of testing to ensure the system performed as expected. The testing plan stages are as below;

- System function and interaction
- Input testing
- Output testing
- Input-output interaction
- Power management

Table 9 is a comparison between transmitters considered for use in this thesis. Outlining key features about each transceiver

Table 9 - Feature Comparison, Synapse [43], Digi International [44].

Feature	RF100PD6	RF200PD1	Xbee 802.15.4	RF301PC1 /	SM700PC 1
Radio manufacturer	Freescale	Atmel	Freescale	Silicon Laboratories	Freescale
Chip set	MC9S08GB60A MCU / MC13191	ATmega128RFA1	MC9S08GT60 MCU / MC13193RF	Si1000 MUC	MC13224V
Frequency Band	2.4 GHz	2.4 GHz	2.4 GHz	868 MHz	2.4 GHz
Raw Bandwidth	250Kbps	2 Mbps	250Kbps	150Kbps	250Kbps
Receive Sensitivity	-102dB	-105dB	-92dB	-99dB	-96dB
Antenna	RP-SMA External	RP-SMA External / F	wire	Chip / U.FL	F / MMCX
Power output	18dB	15dB	0dB	20dB	20dB
Distance (Open Field)	4.8Km	4Km	90m	1.6Km	2Km

Reference List

[1] S. K. Islam and M. R. Haider. (2010). *Sensors and low power signal processing*. Available: http://gateway.library.qut.edu.au/login?url=http://link.springer.com/openurl?genre=book&isbn=978-0-387-79391-7

[2] D. S. Deif and Y. Gadallah, "Classification of Wireless Sensor Networks Deployment Techniques," *Communications Surveys & Tutorials, IEEE,* vol. 16, pp. 834-855, 2014.

[3] "Front Matter," in *Wireless Sensor Networks*, ed: CRC Press, 2012, pp. i-xx.

[4] E. Grenier and D. Humire, "Mesh network planning in urban environments," ATDI Advanced Radio communications2006.

[5] J.-P. Noël and E. Grenier, "Mixed absorption-difraction propergation models for wireless proximity networks," ATDI Advanced Radiocommunications2004.

[6] T. M. David, Gane;, "Vegetation survey of the samford ecological research facility (SERF)," Instatute for Sustainable ResourcesJuly 2010" 2001.

[7] D. Boswarthick, O. Elloumi, and O. Hersent. (2012). *M2M Communications A Systems Approach* [1 online resource (334 p.)]. Available: http://qut.eblib.com.au/patron/FullRecord.aspx?p=875758

[8] N. G. C. G. A. Kameas, "Design guidelines for building a wireless sensor network for environmental monitoring.," pp. 78-80, 2009.

[9] V. Shnayder, M. Hempstead, B.-r. Chen, G. W. Allen, and M. Welsh, "Simulating the power consumption of large-scale sensor network applications," presented at the Proceedings of the 2nd international conference on Embedded networked sensor systems, Baltimore, MD, USA, 2004.

[10] R. Cardell-Oliver, K. Smettem, M. Kranz, and K. Mayer, "Field testing a wireless sensor network for reactive environmental monitoring [soil moisture measurement]" in *Intelligent Sensors, Sensor Networks and Information Processing Conference, 2004. Proceedings of the 2004*, 2004, pp. 7-12.

[11] K. S. J. Pister, "Wireless sensor networks, technology and applications," ed. Berkeley sensor & actuator centre 2007, p. 59:29.

[12] S. Lanzisera, A. M. Mehta, and K. S. J. Pister, "Reducing Average Power in Wireless Sensor Networks through Data Rate Adaptation," in *Communications, 2009. ICC '09. IEEE International Conference on*, 2009, pp. 1-6.

[13] T. Watteyne, S. Lanzisera, A. Mehta, and K. S. J. Pister, "Mitigating Multipath Fading through Channel Hopping in Wireless Sensor Networks," in *Communications (ICC), 2010 IEEE International Conference on*, 2010, pp. 1-5.

[14] R. Lijie, G. Zhongwen, and M. Renzhong, "Distance-based energy efficient placement in wireless sensor networks," in *Industrial Electronics and Applications, 2008. ICIEA 2008. 3rd IEEE Conference on*, 2008, pp. 2031-2035.

[15] "Fresnel zone," ed: Routledge, 1999.

[16] J. Fink, N. Michael, A. Kushleyev, and V. Kumar, "Experimental characterization of radio signal propagation in indoor environments with application to estimation and control," in *Intelligent Robots and Systems, 2009. IROS 2009. IEEE/RSJ International Conference on*, 2009, pp. 2834-2839.

[17] M. Krunz, A. Muqattash, and L. Sung-Ju, "Transmission power control in wireless ad hoc networks: challenges, solutions and open issues," *Network, IEEE*, vol. 18, pp. 8-14, 2004.

[18] A. Muqattash and M. M. Krunz, "A distributed transmission power control protocol for mobile ad hoc networks," *Mobile Computing, IEEE Transactions on*, vol. 3, pp. 113-128, 2004.

[19] H. Karl and A. Willig, *Protocols and architectures for wireless sensor networks*. Hoboken, NJ: Wiley, 2005.

[20] C. Sommer, I. Dietrich, and F. Dressler, "Simulation of Ad Hoc Routing Protocols using OMNeT++," *Mobile Networks and Applications*, vol. 15, pp. 786-801, 2010/12/01 2010.

[21] C. C. P. Anitha, "Comparative Performance Evaluation of Routing Algorithms in IEEE 802.15.4 and IEEE 802.11 with Different Ad Hoc Routing Protocol," *J. Comput. Sci*, vol. 7, pp. 731-735, 2011.

[22] S. S. Harish, Sharma; Santoh, Sahu, "Performance Analysis of DYMO, LANMAR, STAR Routing Protocols for Grid Placement model with varying Network Size," *IJCTA*, vol. 2, p. 2298, 2011.

[23] P. Parvathi, "Comparative analysis of CBRP, AODV, DSDV routing protocols in mobile Ad-hoc networks," in *Computing, Communication and Applications (ICCCA), 2012 International Conference on*, 2012, pp. 1-4.

[24] J. Billington and C. Yuan, "On Modelling and Analysing the Dynamic MANET On-Demand (DYMO) Routing Protocol," in *Transactions on Petri Nets and Other Models of Concurrency III*. vol. 5800, K. Jensen, J. Billington, and M. Koutny, Eds., ed: Springer Berlin Heidelberg, 2009, pp. 98-126.

[25] L. Rongxin, Z. Chaomei, and Z. Yunru, "Study of power-aware routing protocal in wireless sensor networks," in *Electrical and Control Engineering (ICECE), 2011 International Conference on*, 2011, pp. 3173-3176.

[26] J. C. Cano and K. Dongkyun, "Investigating performance of power-aware routing protocols for mobile ad-hoc networks," in *Mobility and Wireless Access Workshop, 2002. MobiWac 2002. International*, 2002, pp. 80-86.

[27] W. Nen-Chung and S. Yu-Li, "A power-aware multicast routing protocol for mobile ad hoc networks with mobility prediction," in *The IEEE Conference on Local Computer Networks*, 2005, pp. 8 pp.-417.

[28] M. Jian, G. Min, Z. Qian, and L. M. Ni, "Energy-Efficient Localized Topology Control Algorithms in IEEE 802.15.4-Based Sensor Networks," *Parallel and Distributed Systems, IEEE Transactions on*, vol. 18, pp. 711-720, 2007.

[29] S. M. Priya and C. C. Sekar, "Energy conserved geo-routing in ad hoc networks," in *Communication and Computational Intelligence (INCOCCI), 2010 International Conference on*, 2010, pp. 72-75.

[30] M. Ishizuka and M. Aida, "Performance study of node placement in sensor networks," in *Distributed Computing Systems Workshops, 2004. Proceedings. 24th International Conference on*, 2004, pp. 598-603.

[31] "lidar," ed: Oxford University Press, 2004.

[32] M. Lemmens, "Airborne Lidar," in *Geo-information*. vol. 5, ed: Springer Netherlands, 2011, pp. 153-170.

[33] K. K. Kemp. (2007). *Encyclopedia of Geographic Information Science*. Available: http://QUT.eblib.com.au/patron/FullRecord.aspx?p=996876

[34] M. Bosse, R. Zlot, and P. Flick, "Zebedee: Design of a Spring-Mounted 3-D Range Sensor with Application to Mobile Mapping," *Robotics, IEEE Transactions on*, vol. 28, pp. 1104-1119, 2012.

[35] H. A. C. LTD. (2014). *UTM-30LX | Product Information | LRF sensors information | HOKUYO AUTOMATIC CO.,LTD.* Available: http://www.hokuyo-aut.jp/02sensor/07scanner/download/products/utm-30lx/

[36] X. Liu, "Airborne LiDAR for DEM generation: some critical issues," *Progress in Physical Geography*, vol. 32, pp. 31-49, Feb 2008 2008.

[37] K. Ali, X. Chen, F. Dovis, D. de Castro, and A. J. Fernandez, "GNSS signal multipath error characterization in urban environments using LiDAR data aiding," in *Satellite Telecommunications (ESTEL), 2012 IEEE First AESS European Conference on*, 2012, pp. 1-5.

[38] C. D. Bonham, *Measurements for Terrestrial Vegetation (2nd Edition)*. Somerset, NJ, USA: John Wiley & Sons, 2013.

[39] (2014). *LAI-2200C Plant Canopy Analyzer | LI-COR Environmental*. Available: http://www.licor.com/env/products/leaf_area/LAI-2200C/

[40] S. R. Wenham, M. A. Green, M. E. Watt, R. Corkish, and A. Sproul. (2013). *Applied Photovoltaics (3 ed.)*. Available: http://QUT.eblib.com.au/patron/FullRecord.aspx?p=1112446

[41] A. Virtuani, E. Lotter, and M. Powalla, "Influence of the light source on the low-irradiance performance of Cu(In,Ga)Se2 solar cells," *Solar Energy Materials and Solar Cells*, vol. 90, pp. 2141-2149, 9/6/ 2006.

[42] "IEEE Standard for Local and metropolitan area networks--Part 15.4: Low-Rate Wireless Personal Area Networks (LR-WPANs)," in *IEEE Std 802.15.4-2011 (Revision of IEEE Std 802.15.4-2006)*, ed, 2011, pp. 1-314.

[43] S. Wireless, "Synapse RF Modules Products: SNAP, instant-on, self-healing, mesh network operating system - www.synapse-wireless.com," 2014.

[44] Digi. (2014, 5/11/2014). *XBee® 802.15.4*. Available: http://www.digi.com/products/wireless-wired-embedded-solutions/zigbee-rf-modules/point-multipoint-rfmodules/xbee-series1-module#specs